Reprinted from

Advances in Molecular Vibrations and Collision Dynamics,
Volume 3, pages 205–248.

ISBN: 1-55938-790-4

With compliments from
Professor Martin Quack
ETH Zürich
Laboratory of Physical Chemistry
CH-8093 Zürich, Switzerland
email: Martin@Quack.ch

SPECTROSCOPY AND QUANTUM DYNAMICS OF HYDROGEN FLUORIDE CLUSTERS

Martin Quack and Martin A. Suhm

ABSTRACT

Hydrogen fluoride clusters $(HF)_n$ and their isotopomers are reviewed as prototype systems for hydrogen bond dynamics. Infrared spectroscopy and ab initio calculations of potential hypersurfaces provide deep insights into the quantum dynamics of the hydrogen bonds in these clusters. Infrared spectroscopic developments using cooled cells, supersonic jets, Fourier transform, and laser techniques have contributed to the progress in our understanding of these clusters, as well as new developments in the analytical representation of empirically refined multidimensional potential hypersurfaces based on many body decompositions. The essential link between potential hypersurfaces and spectroscopic data is provided by quantum dynamical techniques allowing for numerically exact (or almost exact) predictions from solutions of the multidimensional rovibrational Schrödinger equation. The application of quantum dynamical approaches such as quantum Monte Carlo techniques and variational techniques to hydrogen fluoride clusters is summarized. Properties and processes considered include hydrogen bond formation and dissociation, concerted hydrogen bond switching, hydrogen transfer, libration, and intramolecular vibrational–rotational redistribution. Spectral shifts, isotope effects, and the convergence of properties of small clusters to condensed phase properties in large clusters are discussed. We successively review results for the dimer, $(HF)_2$, the trimer, $(HF)_3$, and larger oligomers $(HF)_n$ including finally nanocrystalline clusters with $n >> 100$. Apart from a review of fundamental spectroscopic data we summarize also our current knowledge of the kinetic processes in these clusters, with timescales ranging from femtoseconds to microseconds, as derived from high-resolution spectroscopy.

1. INTRODUCTION

Condensed molecular matter is largely shaped by interatomic and intermolecular forces: fluidity, surface tension, volatility, conductivity, diffusivity, phase state, and hardness—they all depend on how the constituent atoms and molecules interact with each other.[1] Primary processes of cluster dissociation, rearrangement, and

further reactions govern these properties. Their detailed investigation profits substantially from small system sizes. This provides the key incentive for studying isolated molecular clusters in the gas phase. By gradually increasing the cluster size, one can hope to approach condensed phase behavior without having to give up the simplicity of finite systems. Towards the same goal, it is advantageous to choose prototype systems which contain as little nonessential complexity as possible.

Undoubtedly, the hydrogen bond[2] is among the most important intermolecular interactions.[3] Hydrogen fluoride (HF) is the simplest molecule which can undergo such a polar hydrogen bond with itself. In particular the dimer $(HF)_2$ can be and has been studied by high-resolution rotational–vibrational spectroscopy.[4–7] Furthermore, the series of $(HF)_n$ clusters (n = 2, 3, 4, 5, 6, . . .) provides a sequence along which the structure, energetics, and dynamics of the hydrogen bond can be studied particularly well by both experiment and theory.[8] But HF offers additional incentives for a detailed study. Its equilibrium vapor phase exhibits an unmatched clustering tendency at normal temperatures and pressures.[9] In contrast to carboxylic acids,[10] the clustering does not peak at the dimer. Cooperative effects are very pronounced—the interaction energy in a larger cluster exceeds by far the sum of all molecular pair interactions[8] and the dynamics changes accordingly with cluster size. Finally, HF is a powerful solvent[11] for ionic and biomolecular matter and an important etching agent in semiconductor industry.

Experimentally, infrared (IR) spectroscopy provides a sensitive tool for the study of hydrogen bonds.[2,12] Modern supersonic expansion techniques,[13] possibly combined with rovibrational Fourier transform infrared (FTIR) and laser spectroscopy,[14] offer access to hydrogen-bonded clusters in a collision-free environment, while the particular properties of HF also allow a study of these clusters in equilibrium gas cells.[15,16] NMR spectroscopy can provide important complementary information,[17] which has remained largely unexplored for HF in the last decades.[18,19]

On the theoretical side, the small number of electrons in HF allows for high-level electronic structure calculations and for the accurate mapping of multidimensional potential energy hypersurfaces (PES), on which the nuclear dynamics can be investigated.[8] The small reduced mass of the HF molecule together with the pronounced anisotropy of its hydrogen bond interaction typically call for a quantum dynamical treatment,[20] with sizeable quantum effects already at the zero-point level.

The purpose of this review is to summarize some of the recent IR spectroscopic and dynamical insights which have been obtained for clusters of HF from the dimer to nanometer-size aggregates. Rather than being exhaustive, we will highlight a few key dynamical features. A brief review of the connection to thermodynamic properties of the vapor phase has already been published.[9] Other reviews have concentrated on the PES[8,21] and on early dynamical work[21] on HF clusters, or have embedded HF cluster work in a wider framework of molecular aggregates.[22–33] Collisional energy transfer,[21,34] for which accurate dynamical calculations on the most recent PES remain to be done, is not reviewed here. Reviews of some

time-dependent quantum dynamical techniques and symmetry considerations related generally to our work on molecular and cluster dynamics can be found in refs. 35,36.

2. SPECTROSCOPY

Hydrogen bonds convert rotational and translational degrees of freedom into intermolecular vibrations and strongly influence the participating intramolecular X–H stretching modes. Hence, rotational–vibrational spectroscopy is a natural choice for their study. As genuine hydrogen bonds are important in electronegative elements of the first Period (X = N, O, F) with relatively small polarizabilities, linear Raman spectroscopy has not played a dominant role, although it can be useful.[37] The lack of low-lying electronically excited states in HF prevents the application of powerful visible and near-UV laser techniques.[38] Radio-frequency and microwave spectroscopy played an important role in characterizing the HF dimer through its large amplitude tunneling motion[4,39,40] at the start of the era of high-resolution spectroscopy of molecular complexes a quarter century ago. In the future, this frequency range may receive revived interest due to the reliable prediction of vibrationally averaged structures of isotopomeric hydrogen fluoride clusters, which carry a small, zero-point motion-induced dipole moment. For the time being, IR spectroscopy remains the single major spectroscopic approach to elucidate the dynamics of HF clusters. One may distinguish two different techniques:

1. In direct absorption methods, the IR attenuation by the clusters is determined as a function of wavenumber $\tilde{\nu}$. This involves FTIR spectroscopy[6,7,9,16,41,42] as well as diode,[43] difference frequency,[44–47] color center[48,49], and Raman-shifted dye lasers.[50] These techniques provide reliable information about the spectra, including band strengths and linewidths. In favorable cases, the latter may be decomposed into instrumental, Doppler, pressure, and lifetime broadening contributions. Sometimes, sensitivity can be a problem, unless pulsed supersonic expansions[43,44,51,52] or long-path cells[7,16,53] are employed. The sensitivity limits inherent in broadband FTIR spectroscopy have been alleviated recently by using a buffered, synchronously pulsed rapid-scan technique.[9,52] In this method, the full low-resolution (0.2–10 cm^{-1}) IR spectrum is measured in a single rapid scan *during* an intense substance pulse of 50–500 ms duration. The pulse is diluted in a vacuum buffer chamber before entering the mechanical pumping system. By increasing the size of the buffer chamber, the achievable spectral resolution $\Delta\tilde{\nu}$ (determined by the pulse duration t_p via $\Delta\tilde{\nu} = 1/(2t_p v_m)$ where v_m is the mechanical mirror speed) can be increased up to the instrument limits without the need for a larger pumping system. In this way, FTIR jet spectroscopy[54–56] can be applied routinely to molecular clusters in a wide size range.[52]

2. On the other hand, spectroscopies have been employed, which detect the IR absorption indirectly. These include laser-induced fluorescence,[57] bolometric de-

tection,[48,58,59] as well as size-selective scattering and predissociation experiments.[60,61] While bolometric techniques have led to beautifully detailed photofragment distributions for HF dimer,[48] combination with scattering permits discrimination of a given cluster size against all others without requiring rotational analysis (see Section 7). Classical predissociation spectroscopy with mass spectroscopic detection is often misled in its cluster size assignment by extensive cluster ion fragmentation,[62,63] unless it is combined with careful isotope substitution experiments.[64] Double-resonance spectroscopy[65] and saturation spectroscopy[66] have also been applied successfully. Often, these types of spectroscopy have a higher detection sensitivity than direct linear absorption experiments. However, their correct interpretation occasionally requires a detailed knowledge of the available fragmentation channels and typically, they do not resolve the problem of *vibrational* assignment in any better way than direct absorption techniques.

3. POTENTIAL ENERGY HYPERSURFACES (PES)

Our current knowledge about the PES of HF clusters is summarized in a recent review[8]. It derives from two complementary approaches. Ab initio supermolecule calculations at various levels of sophistication[67–69] provide important geometrical and energetical trends as a function of cluster size. Although these trends refer to local minimum energy and saddle point structures rather than to experimentally observable (vibrationally averaged) quantities, they yield qualitative information about the convergence of cluster properties towards the condensed phase.[33] At the highest levels available and for small clusters,[70,71] supermolecule predictions turn out to be even quantitatively reliable in some cases. However, more global PES scans[72] and representations[72,73] are required to *verify* this reliability, because comparison to experimental data involves a nonlocal quantum treatment of the nuclear dynamics (see Section 4). Reliable inversion procedures to obtain a full-dimensional PES from spectroscopic data without quantum-chemical guidance do not seem to be in reach for systems of more than three atoms,[74] thus suggesting the use of large-scale ab initio PES scans. For practical reasons, such scans usually have to be carried out at somewhat lower levels.[72,75] In order to be useful, they require empirical adjustments.[72,76] In order to be applicable to larger clusters as well, they should be based on a many-body decomposition scheme.[8,17,68] The idea is to separate the total energy of the cluster in a given geometry into three or more parts (illustrated here for a pentamer structure, with circles sketching the cluster structure and filled circles denoting those molecules which contribute to a given energy term[8]):

1. The energy of the monomers at the geometry in which they are found in the cluster relative to their free equilibrium energy, the so-called one-body potential V^1. In HF pentamer there are five such terms, each one corresponding to a process:

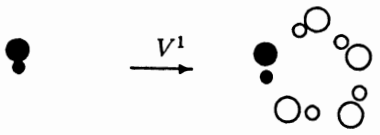

(1)

This monomer relaxation contribution is particularly important for strong hydrogen bonds, such as those present in larger HF clusters. It destabilizes the cluster with respect to the monomers, but this is overcompensated by the stabilization effect on the other contributions at the cluster minimum structure. Often, in a rigid-body framework,[77] this term is neglected.

2. The pair potential V^2, which describes the interaction of *two* monomers in a given (monomer and pair) geometry of the cluster relative to separated monomers in the same monomer geometry. In the pentamer there are ten such terms,[8] each one corresponding to a process:

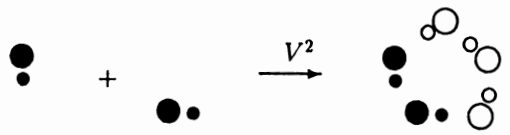

(2)

Typically, the sum over all these pair interactions in a cluster is the most important energetical contribution close to the global minimum structure. Often, it is the only contribution considered at all.[78–80]

3. The three-body potential V^3, which describes that part of the interaction of *three* monomer units in a given cluster geometry which is not captured by monomer relaxation nor by the three pair interactions. In the pentamer there are ten such terms,[8] each one corresponding to a process:

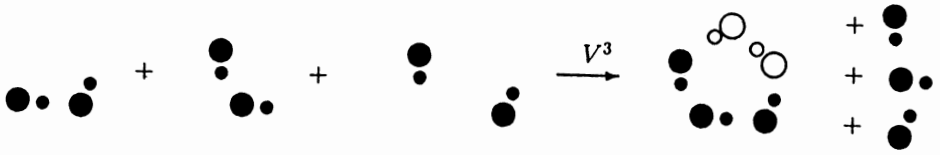

(3)

The three-body potential is often neglected in simplified treatments,[78–81] but it turns out to be essential in hydrogen-bonded systems, reaching up to one-half of the pair interaction in HF clusters at their minimum geometries and much more in some other conformations.[8,17] The popular reduction of the three-body potential to simple induction mechanisms is also not applicable here.[68,82–84]

In principle, further contributions involving four-, five- and higher body forces would have to be included for clusters beyond the trimer. However, their importance typically decreases quickly *after* the three-body term.[8,17,68] They can be neglected altogether for some applications (minimum energy structures, hydrogen bond rearrangements, and energetics at moderate accuracies) or may be restricted to four-body terms in others (highly accurate structures and binding energies, collective vibrations, hydrogen transfer reactions).[8,85]

The first generation of empirically refined full-dimensional pair potentials for HF clusters is represented by the SQSBDE PES,[76] which was mainly based[86] on

systematic ab initio scans by the Vienna group.[75] Currently, the best available pair potentials are SC-2.9 and SO-3, two related, empirically refined fits of more than 3000 high-level ab initio points.[72,87] They are usually combined with a monomer potential of generalized Poeschl–Teller type.[72,87,88] The best available analytical three-body potential HF3BG[8,68,89] is a fit to 3000 ab initio points at lower level without empirical refinement, as the three-body term is relatively insensitive to basis size and correlation treatment. For more details, see ref. 8.

4. QUANTUM DYNAMICAL APPROACHES

The connection between these potential energy surfaces and spectroscopic results[14,90] requires a careful characterization of the multidimensional dynamics of HF clusters. The cluster sizes discussed here range from the tetratomic dimer to nanometer-scale aggregates. The applicable dynamical methods depend very critically on this size. While complete full-dimensional bound state and quantum scattering calculations are only in reach for a pair of diatomics, the largest of these clusters can at most be treated at a locally harmonic or classical dynamical level, except for maybe the quantum ground state. Figure 1 schematically orders some of the available methods according to their applicability to HF clusters of increasing size.

We shall give a very brief outline of the possibilities and limits of some of the more important methods which have been applied to HF clusters, before presenting results for individual cluster sizes.

4.1. Variational Techniques

For low-dimensional problems, rigorous variational techniques using finite basis set or discrete variable representations of the complete configuration space are very powerful.[91,92] Applications to clusters of two flexible diatomic molecules (six vibrational degrees of freedom) represent the state of the art in this field[93] and can provide a very accurate description of the bound and metastable state dynamics of $(HF)_2$,[94–96] including photofragment formation and distribution.[97–99] Collocation methods have been used as well.[100] For larger systems, selective diagonalization techniques are useful.[101–104]

From the rigorous variational approaches, a series of approximate methods can be derived. For the HF dimer, a powerful approximation consists in adiabatically separating the two high-frequency monomer vibrations from the four low-frequency hydrogen bond modes.[16,72,105–108] The resulting (4 + 2)D adiabatic wavefunctions retain the full dimensionality of the problem but can be obtained much more economically. This also allows for an efficient and accurate treatment of rotationally highly excited states,[72,107,108] which are currently too demanding for rigorous treatments. Limitations of the adiabatic approach will be discussed in Section 5.

In a "crude adiabatic" (4D) approach,[16] the monomer degrees of freedom are kept fixed at their equilibrium value or at some effective, vibrationally averaged geome-

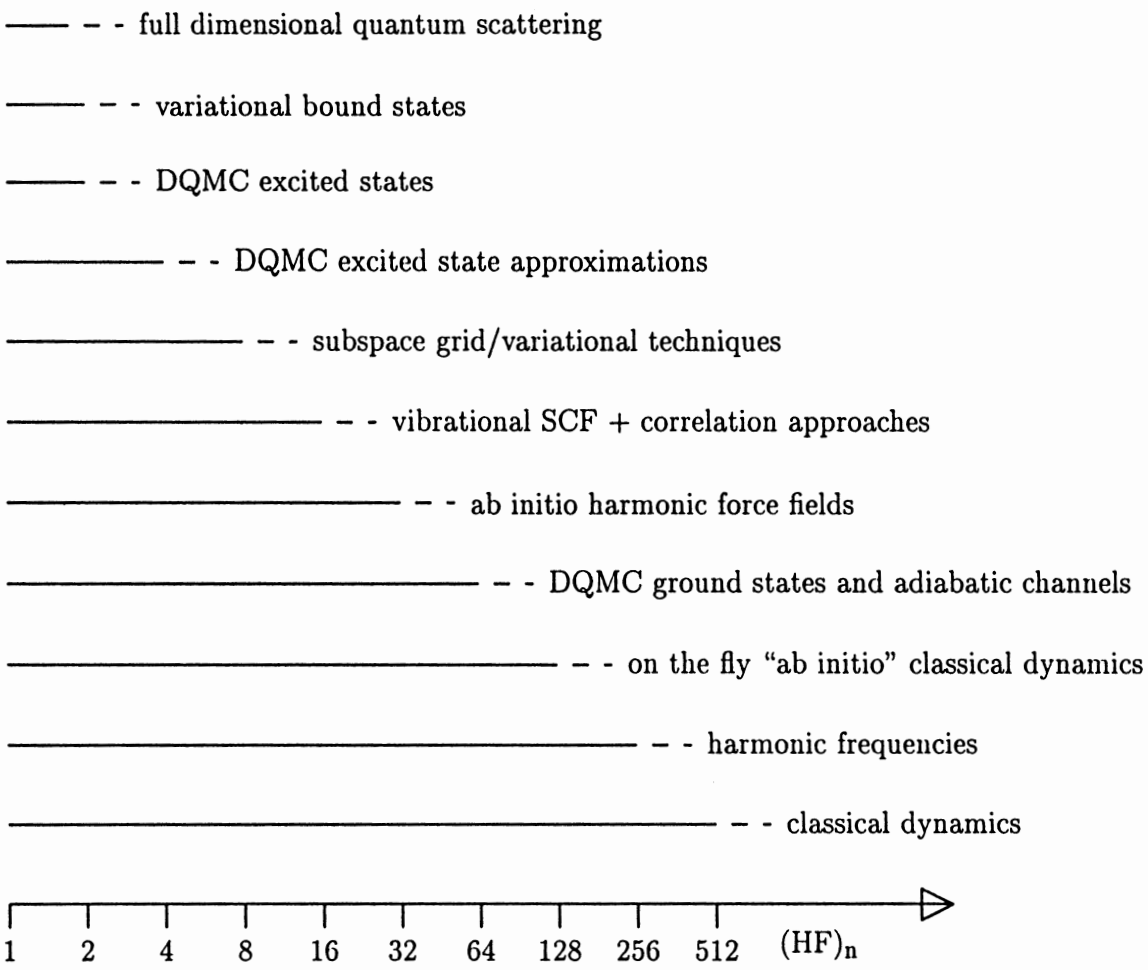

Figure 1. Approximate ordering of various dynamical methods according to their applicability to HF clusters $(HF)_n$ of increasing size n.

try.[109,110] While this introduces some arbitrariness, it is a reasonable assumption for weakly interacting monomers if one is mostly interested in the van der Waals modes. HF dimer is a borderline case, whereas larger HF clusters interact too strongly to make this a very useful assumption.[8] For larger molecules such as water and ammonia, the rigid monomer approach is often a prerequisite for the application of variational techniques and for the availability of suitable interaction PES.[90,104,111]

In larger HF clusters, where a full variational treatment is out of reach even for frozen monomers, one can clamp further coordinates and concentrate on reduced subspaces. Such approaches have also been applied to $(HF)_2$,[112] where one can check their reliability against more rigorous treatments. Investigations of the n-dimensional pure HF stretching subspace for $(HF)_{n<6}$[42] and of the three in-plane or the three out-of-plane librations for $(HF)_3$[65] have given important insight into subspace anharmonicities and have supported experimental assignments. However, great care is indicated in such treatments, since anharmonic contributions of the

neglected low-frequency modes can be very substantial, in particular when one deals with dissociative degrees of freedom.[31,76,113] In such cases, it is advisable to include at least the zero-point energy of the bath modes, i.e. to treat the subspace dynamics on an adiabatic surface.

Rather than freezing certain degrees of freedom, one may consider a variational self-consistent-field representation of the coupled modes,[114,115] which is so successful in the field of electron dynamics. First results along these lines, including also the perturbation treatment of neglected mode correlations, are quite promising,[114] but rigorous tests for well-characterized cluster systems such as HF dimer remain to be carried out.

Finally, one may ask whether one-dimensional variational treatments may be useful for such hydrogen-bonded clusters. The high symmetry and strong coupling in the HF ring complexes leaves relatively little room for a meaningful one-dimensional coordinate choice, unless the symmetry is broken via isotopic substitution.[52] In HF dimer, one can in fact devise one-dimensional paths for dissociation and hydrogen bond interchange, but simplified treatments of the dynamics along these paths[116,117] seem to lead to erroneous results. Again, a minimum requirement appears to be inclusion of the zero-point energy contributions of neglected bath modes.[76,118] This leads us to a completely different class of dynamical methods, which are dealt with in the next sections.

4.2. Diffusion Quantum Monte Carlo (DQMC) Techniques: The General DQMC Approach for Ground-State Properties

Even if the essential dynamical aspects of a molecular cluster are born out of a restricted subspace of the PES and can thus be treated with variational methods, there will typically be nontrivial zero-point energy contributions of the remaining modes. Neglect of these contributions will lead to systematic errors in the comparison between experiment and theory. For hydrogen-bonded systems, such errors are particularly large, because the spatial containment of the light hydrogen in the intermolecular bond gives rise to a sizeable spread in momentum.

The diffusion quantum Monte Carlo approach[119–125] provides a rigorous and simple method to evaluate the zero-point energy E_0 and wavefunction ψ_0 of arbitrary subspaces (including the full configuration space) up to very large cluster sizes, given the potential energy hypersurface V. The method relies on an isomorphism between the N-particle time-dependent Schrödinger equation for nuclear motion (masses m_k), when written in terms of an imaginary time equivalent $(it/\hbar = \tau)$,

$$\frac{\partial \psi}{\partial (it/\hbar)} = \left(\sum_{k=1}^{N} \frac{\hbar^2}{2m_k} \nabla_k^2 - (V - E_R) \right) \psi \tag{4}$$

and a multidimensional transport equation for ψ:

$$\frac{\partial \psi}{\partial \tau} = \left(\sum_{k=1}^{N} D_k \nabla_k^2 - (V - E_R) \right) \psi \tag{5}$$

The wavefunction ψ is mimicked by a discrete distribution of random walkers which undergo multidimensional anisotropic diffusion with diffusion coefficient D_k in coordinate space and a first-order growth/shrinkage process according to the local potential energy V, shifted dynamically by a coordinate-independent term E_R. For long (imaginary) times, a stochastic stationary distribution of the random walkers can be reached. It corresponds to the ground state wavefunction ψ_0 of the cluster (or a given subspace), and the potential energy shift E_R required to achieve stationarity is equal to the numerically exact cluster ground state energy E_0, to within a symmetrical error bar which results from the stochastic nature of the simulation.

When applied in cartesian coordinate space without any restrictions, the DQMC method can be used to predict the spectroscopically observable dissociation energy D_0 of the cluster, which is linked to the electronic dissociation energy D_e, via,

$$D_0 = D_e - \Delta E_0 \tag{6}$$

where ΔE_0 is the difference in zero-point energies between the cluster and its fragments. Such accurate dissociation thresholds are important for the correct interpretation of predissociation experiments and for the thermodynamics and kinetics of evaporation and condensation.

4.3. Symmetry Restricted DQMC Approach for Excited States

Another DQMC application arises when the multidimensional configuration space of the cluster is divided *symmetrically* by a given hypersurface and random walkers are killed whenever they attempt to cross the hypersurface. In this way, one can generate a wavefunction which is antisymmetric with respect to this hypersurface.[122,126,127] Usually, the hypersurface can be distorted in one or more dimensions without destroying its symmetry.[128] In such a case, the algorithm will generate an upper bound of the exact lowest antisymmetric eigenstate of the cluster. In rare (low-dimensional) cases, the dividing (nodal) surface is *completely* defined by symmetry and an exact excited eigenstate is obtained. For instance, a cluster of four ordered atoms will be either planar, left-handed, or right-handed with respect to some stereochemical convention. The hypersurface of all planar configurations separates left- from right-handed clusters and is fully determined by this symmetry requirement alone. In such a case, the quantum Monte Carlo method can be used to obtain the corresponding lowest symmetric and antisymmetric eigenstates without approximation. If the nodal surface of a given cluster vibrational state is known approximately, e.g. from an SCF calculation,[114,115] DQMC can be used to obtain *better* estimates of cluster eigenstates using this fixed node.[129] Furthermore, the nodal surfaces can be optimized in order to improve the eigenvalues further.[68,127,130,131]

4.4. Quasiadiabatic Channel Quantum Monte Carlo Method for Rotationally and Vibrationally Excited States

If the random walk is constrained to a subspace of the full configuration space, it yields the zero-point energy of this subspace alone, which could be the space of bath modes in a restricted variational calculation.[76,118] For example, one can solve the Schrödinger equation for the nuclear motion in a cluster such as HF dimer for clamped HF···HF distance R. The resulting eigenvalues of the Hamiltonian as a function of R define adiabatic channels,[113,132] which are important for statistical theories of reaction kinetics. The DQMC algorithm can be used to accurately calculate the lowest adiabatic channel for reactions of nearly arbitrary complexity, e.g. for enzyme reactions, if an analytical PES is available. In simple cases, symmetry also allows for the calculation of excited channels in the spirit of the previous section. An example for HF dimer, where the lowest channel of each

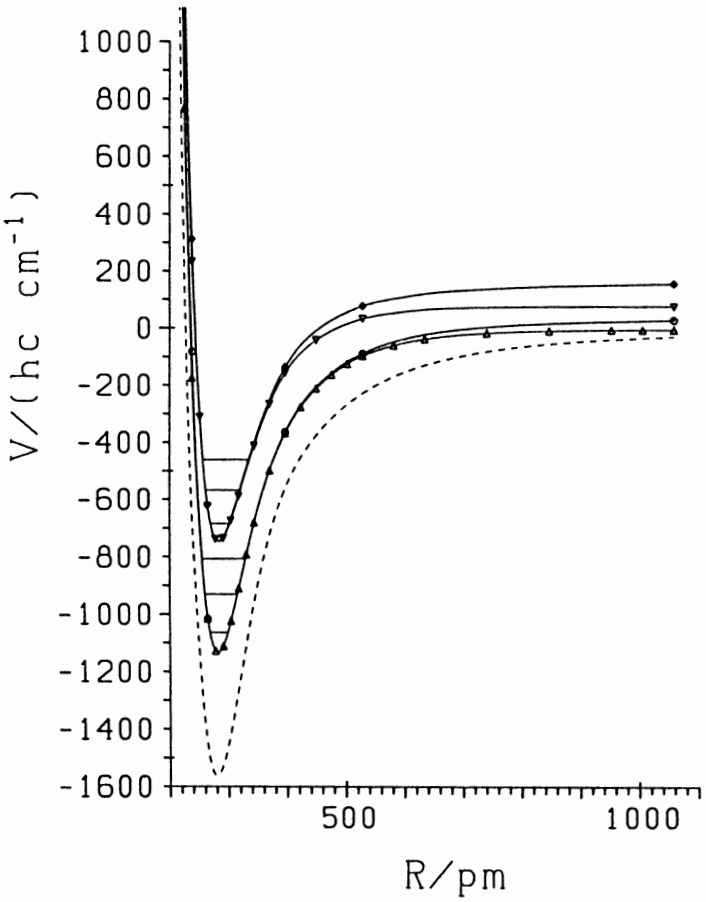

Figure 2. Lowest quasiadiabatic DQMC dissociation channels of each symmetry (full lines with symbols, A^+, B^+, A^-, B^- from bottom to top) for HF dimer together with the minimum energy path (dashed curve).[76] The channel energies are shown with respect to two separate HF monomers in their lowest quantum states and the minimum energy path goes to 0 for large R.

symmetry has been calculated, is given in Figure 2. Within such adiabatic channels, the 1D Schrödinger equation for motion along R can be solved using standard techniques[133,134] to yield reliable stretching eigenvalues within the adiabatic approximation. Some of these eigenvalues are indicated by horizontal lines in Figure 2.

The DQMC algorithm can also be applied to effective rotational surfaces, which are obtained from the electronic potential energy by locally adding rigid rotor term energies. In this way, vibrationally averaged rotational constants and other expectation values[76,135,136] can be calculated[76] and compared to experiment. By combining the clamped R approach with effective rotational surfaces, dissociation channels with overall angular momentum can be obtained by DQMC. Three such channels for different J are shown in Figure 3.

The strategy of *empirical refinement* of PES via DQMC calculations of rotational constants and spectroscopic dissociation energies, which we introduced in reference 76, is now applied frequently,[72,127,137–139] and testing of van der Waals PES with DQMC runs has almost become routine[140] since its first applications.[141] It should be emphasized[135,142–144] that expectation values of the rotational constants are not necessarily identical to the spectroscopically defined rotational constants.

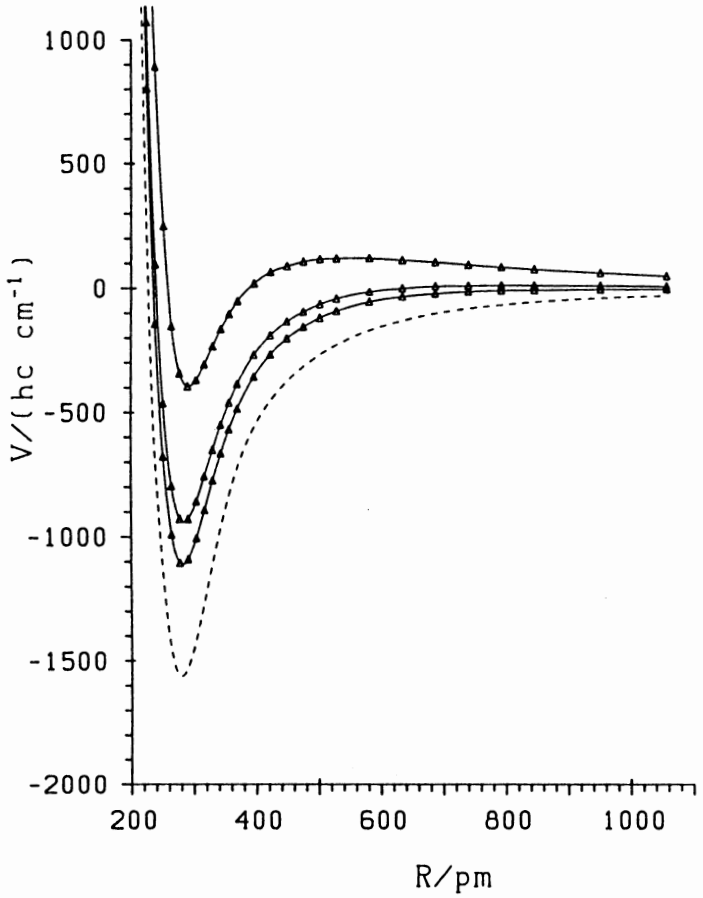

Figure 3. Lowest quasiadiabatic DQMC dissociation channels for total angular momentum J = 10, 30, and 60 for HF dimer together with the minimum energy path (dashed curve).[76]

The main advantage of the DQMC method over basis set approaches is its favorable scaling with system size, which it has in common with other Monte Carlo techniques, and the numerically exact nature of the result for selected vibrational states. Beyond the determination of vibrationally averaged cluster structures and dissociation energies, which are important for the interpretation of spectroscopic predissociation measurements, DQMC is most powerful in combination with variational subspace treatments, to which it can add the zero-point energy of the neglected bath modes in an adiabatic framework.[76]

4.5. Classical and Harmonic Approximations

If global PES are available but quantum dynamical treatments are out of reach, one can resort to classical dynamical treatments. As discussed, one should be aware of sizeable errors for HF and other hydrogen-bonded systems in this case. In early applications to liquid HF[78,145] and HF clusters,[79] the error in the (pairwise additive) PES was at least comparable to that of the classical approximation and the two tend to partially compensate each other.[9] The classical dynamical treatment of HF clusters in Ar matrices has been applied for estimates of matrix shifts.[146] One may also consider to embed a local quantum subsystem into a classical solvent environment, but this will be less advantageous in a homogeneous HF cluster.

On the fly dynamical evaluations or "ab initio molecular dynamics"[147,148] circumvent the need for an analytical PES but they are still limited to relatively inexpensive and consequently approximate electronic structure approaches, usually density functional theory.[149,150] Nevertheless, they have provided valuable theoretical insights into the structure of liquid HF.[151] The inclusion of thermal quantum effects via path integral approaches[152,153] would be particularly attractive for the hydrogen fluoride system due to its pronounced librational quantization.

If sufficiently accurate global PES are not available but a rough dynamical characterization of the cluster is required, one can resort to the local harmonic approximation, which is included as a standard option for many electronic structure approaches in quantum chemistry codes both for minima in the potential and for saddle points (transition state structures). Due to the correspondence between quantum and classical harmonic oscillators, such a quadratic force-field diagonalization is equivalent to low-temperature classical dynamics simulations. The harmonic approach will miss out important features of large amplitude motion such as tunneling splittings,[4] pronounced anharmonicities,[42] overtone and combination bands,[14] and anomalous isotope effects[31,76,118] but it provides a qualitative picture of the fundamental spectrum for the more strongly bound HF clusters and—most importantly—of cluster-size trends. Also, the harmonic force field is a reasonable meeting point between empirically refined analytical potential energy surfaces and high level ab initio benchmark calculations which would be too expensive for systematic surface scans.[71,154] Quite often, substantial error compensation between various anharmonic effects contributes to the apparent success of the harmonic

approximation (see Section 7.2), but when this cancellation is understood through careful anharmonic analysis, it can even be exploited for predictions of spectroscopic properties.[41,42,52] Recently, we have developed an efficient quasiadiabatic channel approach for polyatomic molecule spectroscopy, treating many degrees of freedom quasiharmonically.[248] This approach may sometimes be useful for large clusters, involving possibly large polyatomic molecules as monomer units.

5. SPECTROSCOPY AND DYNAMICS OF THE DIMER $(HF)_2$ AND ITS ISOTOPOMERS

Among all HF clusters, the dynamics of the dimer has been characterized in most detail. We will first summarize observed vibrational states of this complex in comparison to theory and then concentrate on the discussion of some key primary processes in this prototypical system, namely the hydrogen bond interconversion process, the dissociation process and the librational dynamics.

5.1. Rovibrational States of $(HF)_2$: Spectroscopy and Theory

The character and nomenclature of the six vibrational modes of HF dimer have been summarized before.[76] Basically, the modes occur in three pairs. At the low-frequency end, there is a pair of bend (ν_5)[7] and FF stretch (ν_4)[76] vibrations, whose degree of mixing is sensitive to details of the potential energy surface and isotopic substitution.[46,72,76,155] A pair of librations (ν_3, ν_6)[6,47,72,76] occurs at higher frequency in the far-infrared, and will be discussed in Section 5.4. Finally, there is a pair of high-frequency HF stretching modes (ν_1, ν_2)[5,16,53,72,76,156] whose excitation by one or more[16,43,44,57,157] quanta systematically affects the low-frequency hydrogen bond dynamics.[16,46,47] Our direct experimental knowledge about the hydrogen bond modes and rotation around the FF axis with K quantum number is summarized in Figure 4.[7] It has been confirmed and extended by the investigation of hydrogen bond modes in combination with HF stretching vibrations.[46,47]

With the help of recent accurate PES and dynamical methods, many spectroscopic details can be reproduced and understood, while others can be predicted. Table 1 gives a selection of level predictions in comparison with experiment. In particular, the performance of a recent ab initio PES (G_{R12}|R12-CP) and its empirical refinement (G|SC-2.9), the performance of the (4 + 2)D adiabatic separation compared to a full 6D treatment, and the performance of earlier PES (SQSBDE and SNB) can be judged. Details are discussed elsewhere[72,87,96,107,108] and in the following sections.

5.2. Hydrogen Bond Interconversion

Hydrogen bond interconversion in HF dimer, schematically represented by,

$$H^{(1)}\!\!\searrow\!\!F \cdots H^{(2)}\!\!-\!\!F \rightleftharpoons F\!-\!H^{(1)} \cdots F\!\!\searrow\!\!H^{(2)} \qquad (7)$$

has been considered as one of the central primary processes of cluster dynamics ever since its first characterization a quarter century ago through the observation of a tunneling-split ground state[4] with a splitting of $\Delta\tilde{\nu}_T = 0.658690\ cm^{-1}$. The one-dimensional disrotatory potential trough along which the exchange occurs is rather well-established,[53,116,118,158] but the tunneling dynamics is not determined by

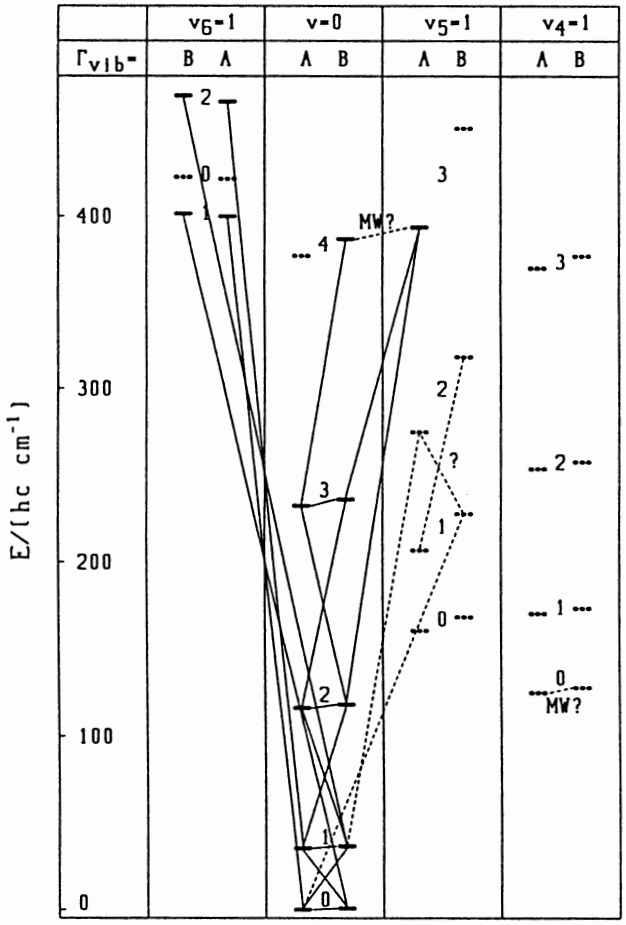

Figure 4. Energy level scheme for experimentally characterized $(HF)_2$ *K* sublevels of hydrogen bond modes in the far-IR,[7,193] complemented by some theoretical predictions. Horizontal bars indicate levels which have been assigned via rovibrational transitions (marked as connecting lines). Dashed bars mark levels which are tentatively assigned (via transitions which are shown as dashed lines) or predicted. Predictions of microwave transitions are also shown as dashed lines (MW). The *K* quantum number is indicated between the pairs of tunneling sublevels (Γ_{vib} = A, B).

Table 1. Selected HFHF Anharmonic Transition Wavenumbers (in cm^{-1}) from Experiment and Theory[a]

Vibration	K	Experimental	*GISC-2.9 (4+2)D (ref. 72, 87)*	*G_{R12}IR12-CP (4+2)D (ref. 72, 87)*	*SQSBDE (4+2)D (ref. 105)*	*SQSBDE 6D/{4D} (ref. 94, 95)*	*SNB[68] (4+2)D (ref. 105)*
$D_0/,hc$	0	1062[176]	1062	1000	1058	1057[d]	1062
$\Delta\nu_T(\nu_0)$	0	0.659[118,247]	0.61	0.65	0.45	0.44	0.66
ν_0	1	35.425[53,118]	37.7	37.1	39.4	{39.9}	38.5
$\Delta\nu_T(\nu_0)$	1	1.064[247]	1.03	1.00	0.78	{0.86}	1.15
ν_0	2	116.133[53,118]	120.6	119.7	125.2		122.1
$\Delta\nu_T(\nu_0)$	2	2.004[118]	2.13	2.00	1.64		2.42
ν_0	3	232.632[118]	238.9	238.2	246.3		239.9
$\Delta\nu_T(\nu_0)$	3	3.813[118]	4.23	3.89	3.59		5.21
ω_4 ('stretch')			155	156	151	151	150
ν_4	0	125(5)[76]	126.3	125.3	126.4	126.4	125.1
$\Delta\nu_T(\nu_4)$	0	>2[76]	2.88	2.56	1.00	0.98	1.70
ω_5 ('bend')			209	207	211	211	203
ν_5	0	≈161[7]	163.7	162.3	161.2	160.6	151.9
$\Delta\nu_T(\nu_5)$	0		7.60	7.64	7.65	7.48	9.59
ν_4	1		173.8	171.9	168.5	{167.9}	166.7
$\Delta\nu_T(\nu_4)$	1		2.85	2.36	1.27	{1.45}	1.95
ν_5	1		210.1	209.0	215.7	{214.3}	202.9
$\Delta\nu_T(\nu_5)$	1		19.3	18.4	17.9	{18.7}	22.4
ν_5	3	393.550[7]	396.6	396.8	400.9		382.4
ω_6 (oop libr.)			467	465	401	401	409
ν_6	0	≈380[c]?[106]	422.2	419.4	379.4	378.7[b]	378.0
$\Delta\nu_T(\nu_6)$	0		2.28	2.37	2.13	1.75[b]	2.56
ν_6	1	399.79[6]	399.3	397.3	361.7	{360.4}	358.2
$\Delta\nu_T(\nu_6)$	1	1.625[6]	1.24	1.33	5.53	{5.82}	3.59
ω_3 (ip libr.)			547	544	485	485	484
ν_3	0		483.1	479.8	426.1?	425.3?	415.3?
$\nu_3 + \Delta\nu_T$	0		?	?	440.9	440.3?	434.0
ω_2 (bound HF)			4030	4013	4048	4048	4055
ν_2	0	3868.1[53]	3867	3854	3896	3896	3867
ω_1 (free HF)			4094	4087	4100	4100	4099
ν_1	0	3930.9[53]	3924	3920	3938	3941	3930
ν_2	1	3900.6[53]	3902	3888	3935		3907
ν_1	1	3962.9[53]	3960	3954	3976		3964
$N = 2$	0	7555(15)[16]	7543	7516	7639	7643	7551
(triad)[16]	0	7682.8[43,44]	7670	7662	7706	7714	7683
	0		7790	7773	7839	7842	7798
$\nu_4 + \nu_2 - \nu_2$	0	132.616[46]	132	132	135	138.5	127
$\nu_4 + \nu_1 - \nu_1$	0	127.573[46]	126	125	127	124.2	129
$\nu_4 + \nu_1 - \nu_1$	1	169.521[46]	172	170	168		170
$\nu_5 + \nu_2 - \nu_2$	0	178.667[46]	174	175	166	169.6	160
$\nu_5 + \nu_2 - \nu_2$	1	220.615[46]	219	219	221		204
$\nu_5 + \nu_1 - \nu_1$	0	166.523[46]	165	163	159	160.7	155
$\nu_6 + \nu_2 - \nu_2$	1	425.690[47]	421	423	370		?
$\nu_3 + \nu_1 - \nu_1$	0	487.015[47]	485	482	420		418?

Table 1. continued

Notes: [a]$\Delta\nu_T$ denotes tunneling splittings, harmonic wavenumbers ω are given for comparison. The adiabatic (4+2)D approach is described and refined in refs. 107,108. Some ν_3 assignments (marked ?) are difficult due to extensive mode mixing. See text and ref. 72 for details.
[b]Accurate DQMC calculations[72] give ν_6 = 378.6(8) cm^{-1} and $\Delta\nu_T(\nu_6)$ = 1.85(30) cm^{-1}
[c]probably too low by ≈40 cm^{-1}, see section 5.4
[d]DQMC gives D_0/hc = 1057.5(0.5) cm^{-1} on the SQSBDE surface.[105]

the barrier height alone. The width of the barrier and the coupling to the other vibrational modes are equally important, as illustrated in Figure 5. Even for closely related PES such as the series R12-CP/SC-2.9/SO-3, the correlation between barrier height and tunneling splitting is counterintuitive. Rather than increasing with decreasing barrier height, the tunneling splitting $\Delta\tilde{\nu}_T$ even increases in the sequence. Other things remaining equal, the tunneling splitting will of course increase monotonically with decreasing barrier, until it converges to the appropriate free rotor level spacing. But this one-dimensional argument does not apply for a fully coupled potential. Empirically adjusted PES such as S2,[159,160] and to lesser extent the SNB[8,68,105,106] and the 4D BH[53,109] potential, have considerably lower barriers than ab initio calculations of appropriate quality.[72,87] Nevertheless, the predicted tunneling splittings are similar (Figure 5), while the recent ab initio based PES are much more successful for other experimental data.[72]

The calculation of the ground-state tunneling splitting $\Delta\tilde{\nu}_T$ on 6D PES of HF dimer was first achieved via DQMC methods,[76,120] which provide a tight upper bound for this quantity,[105] as the wavefunction node is *nearly* exclusively determined by symmetry.[118] However, these results carry a relatively large statistical error bar ($\Delta\tilde{\nu}_T$ = 0.4 ± 0.4 cm^{-1}, 0.45 ± 0.15 cm^{-1} for the SQSBDE surface[76,105]) unless correlated sampling techniques are employed.[161,162] For rigid monomers, i.e. on the 4D intermolecular PES, the excited wavefunction node is given exactly by symmetry, so that rigorous DQMC calculations are possible.[118] This can be exploited in rigid-body DQMC calculations[163] of molecular clusters,[164] but in each case, one has to check carefully whether the node is really determined by symmetry alone. The 4D tunneling splitting of HF dimer has also been evaluated variationally[97,107,109,110] in good agreement with the 6D and 4D DQMC results.[105] Highly accurate 6D ground-state tunneling splittings for HF dimer have become available recently[94,96,160] and confirm that the *monomer* zero-point motion has a rather small influence on the interconversion rate.

With respect to hydrogen bond interconversion, HF dimer is clearly in the high barrier limit. The ground-state splitting amounts to less than 2% of the low barrier limit of $2B_0$,[76] where B_0 is the rotational constant of an HF molecule. Therefore, one expects that rovibrational excitation can have pronounced effects on the splittings and the experimental characterization of these effects is an ongoing

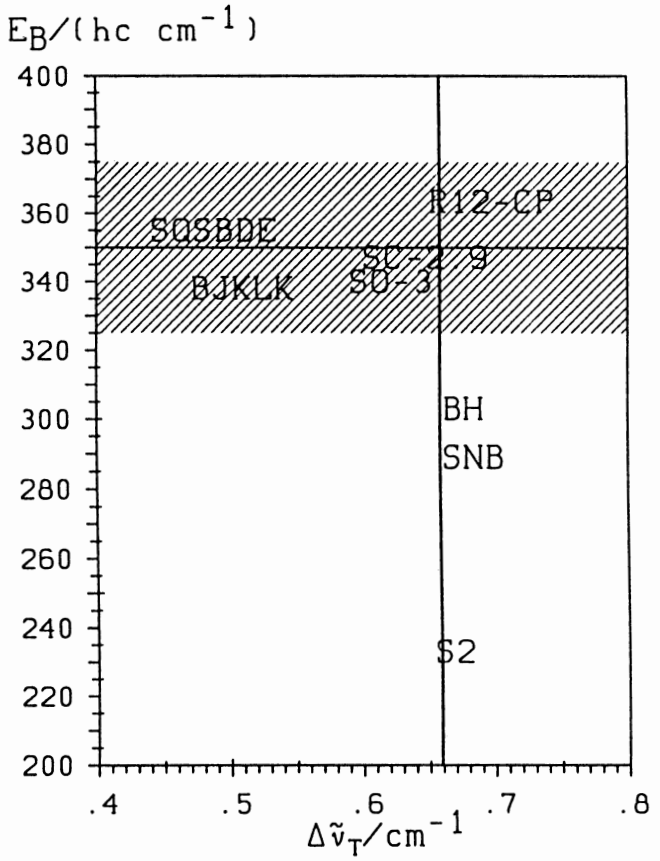

Figure 5. Correlation of the $(HF)_2$ ground-state tunneling splitting $\Delta\tilde{\nu}_T$ with the electronic barrier height E_B of hydrogen bond interconversion (Eq. 7) for various analytical PES. The lower left corner of the labels marks the corresponding values for the BJKLK,[117,159] SQSBDE,[76,94] R12-CP,[72] SC-2.9,[72] SO-3,[87] BH,[53,109] SNB,[8,68,105,106] and S2[159,160] potential energy hypersurfaces. The solid vertical line gives the experimental tunnelling splitting[4,118] and the hatched area denotes the currently best estimate for the barrier height.[72]

challenge. Excited-state tunneling splittings known up to 1989 have been summarized before.[16,165] Figure 6 contains an updated graphical compilation up to the first HF stretching overtone (see also Table 1).

For the definition of the sign of the tunneling splitting we use the *total* vibrational symmetry of the state, Γ_{vib}, which can be either symmetric (A) or antisymmetric (B) with respect to monomer exchange (in addition to + or – parity[6,166]). The splitting is defined as the energy of the B state minus the energy of the A state. Separation of the vibrational symmetry Γ_{vib} into a contribution from the HF stretching symmetry $\Gamma_{stretch}$ and a contribution from the tunneling symmetry Γ_{tun} is possible in theoretical calculations but by no means trivial from a purely experimental point of view.[16,43,44,107,108,156]

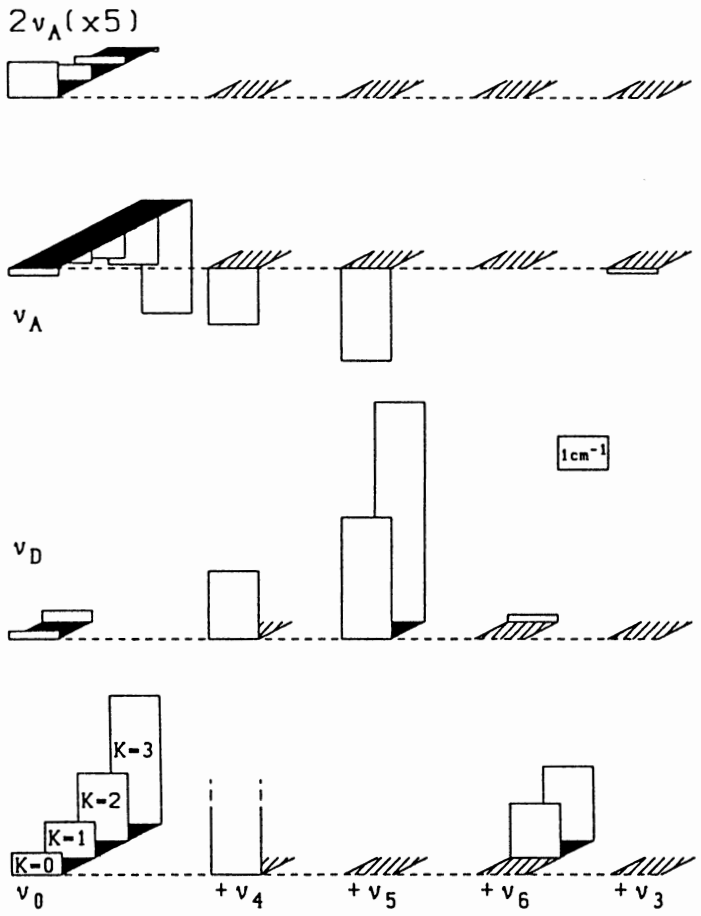

Figure 6. Trends[16,165] in experimentally measured tunneling splittings $\nu_{\Gamma_{vib=B}} - \nu_{\Gamma_{vib=A}}$ (vertical bars proportional to the splitting) as a function of hydrogen bond excitation (ν_4, ν_5, ν_6, ν_3, from left to right), as a function of HF stretch excitation (ν_D, ν_A, $2\nu_A$, from bottom to top) and as a function of rotational excitation around the A axis (quantum number $K = 0 \ldots 4$, from front to back, indicated by horizontal hatched bars in perspective view). Black horizontal bars connect measured levels of the same vibrational state with different K, i.e. those which allow for a K-dependence analysis of the splitting. Downward vertical bars indicate negative tunneling splitting (Γ_{vib}), due to either antisymmetric stretch excitation ($\Gamma_{stretch}$ = B, as in ν_A) or due to an inverted hydrogen bond exchange doubling (Γ_{tun} = A above Γ_{tun} = B). The $2\nu_A$ results[43,174] are magnified 5-fold to show the subtle switchover of tunneling sign between $K = 2$ and $K = 3$. Results for the tetrad with 3 HF stretching quanta[16,57,157,167] are not shown.

As illustrated in Figure 6, important gaps remain to be filled for hydrogen bond fundamental vibrations.[6,7,76] The ν_4 tunneling splitting has been experimentally estimated to be larger than 2 cm^{-1} from a vibrational ground-state perturbation analysis.[76] For the ν_5 vibration, only one tunneling level for $K = 3$ could be assigned.[7] HF stretching fundamentals (ν_D, predominantly involving the donor molecule, and ν_A, mainly involving the acceptor stretch),[16,53] first[16,43,44] and second overtones[16,57,167] are relatively well-characterized, although one member of each overtone polyad remains undetected.[43,157] Recently, several hydrogen bond vibrations built on HF[46,47] and DF[168] stretching fundamentals have been measured and interpreted. While the results provide valuable predictions for the location of pure hydrogen bond vibrations in the far-infrared and information on the inter–intramolecular coupling, the splittings cannot be easily extrapolated to the HF stretching ground state. This has to do with a general hindrance of the interconversion process by monomer excitation[16,53] (see Figure 6), also found in other dimers.[169,170] Several mechanisms for this vibration-induced slowdown of tunneling have been proposed.[16,21,53,158,167,169,171,172] Basically, these fall in two categories:

1. HF stretching excitation stabilizes the dimer, as directly evidenced by the shift of the corresponding monomer vibrations to lower frequencies in the cluster.[16,53] This stabilization may be less pronounced near the interconversion barrier, hence leading to a larger barrier and a smaller tunneling splitting.[173] Adiabatic (4 + 2)D calculations on existing potential energy surfaces do not seem to support this interpretation. While there are adiabatic barrier effects, they are not sufficiently pronounced nor are they systematically *reducing* the splitting.[107] Furthermore, full 6D calculations[95] on the same PES suggest that the splitting reductions must be also due to other effects. The situation is by no means simple because of many possible definitions of effective adiabatic tunneling potentials.

2. During interconversion, HF stretching excitation has to be transferred from one monomer to the other (see Eq. 7). This leads to adiabatic diagonal corrections[158] and diabatic effects[169] whenever the two monomers are excited by *different* amounts. In essence, the character of the wavefunction changes quickly in the vicinity of the barrier, introducing an additional dynamical bottleneck. An excellent experimental test of this model might be the as yet unobserved tunneling splitting in the state with one HF stretching quantum in each monomer,[16,43] which should only exhibit adiabatic effects relative to the ground-state splitting of 0.66 cm^{-1}. 6D calculations indeed predict this splitting to be relatively large[95] for the SQSBDE surface. Furthermore, a state with three stretching quanta *distributed* over the two monomers[57] exhibits a substantially larger experimental tunneling splitting than states where all three quanta are localized in one monomer.[57] It seems possible, and perhaps even likely, that both effects, the general tightening of the hydrogen bond and the extra dynamical effects due to restricted vibrational energy exchange, as

well as other, more complicated phenomena, contribute to the reduction of the tunneling splitting upon HF stretching excitation.

Building upon the early observations of the $N = 1$[53] and the $N = 2$ and 3 polyads,[16] several groups have recently contributed to experimental progress in measuring various HF stretching excited levels and tunneling splittings.[43,44–47,57,67,174] The experimental situation is thus fairly clear. However, there seems to be no simple model predicting the experimental observations.

The accurate prediction of tunneling splittings in these highly excited states is a considerable challenge. This includes the analytical PES representation, as relatively subtle couplings are involved. In some cases, such as for the state with two quanta in the free HF stretch,[16,43,44] the tunneling splitting is even *reversed* with respect to several earlier theoretical calculations.[44,72,95,107,156] A sufficiently refined PES should be able to reproduce and explain this qualitative anomaly, which depends on the K-rotational state[16,43,44,174] (see Figure 6) and for which possible causes have already been discussed.[16,44] The exact quantum dynamics on the recently published SO-3 potential[87] seems to correctly reproduce the experimental observations,[96] which have defeated the previous attempts of simpler explanations.

Although tunneling splittings are particularly sensitive probes of the accuracy of a PES, one should not rely exclusively on them. For example, the empirically refined SO-3[87] and SC-2.9[72] surfaces, the purely ab initio BJKLK surface,[117] and the S2 surface,[151] which was refined specifically along the tunneling coordinate, all perform quite similarly for a set of six known tunneling splittings with various degrees of HF stretch excitation.[96,159] However, the BJKLK and, in particular, the S2 surface are too flat in the librational degrees of freedom. Furthermore, the S2 surface[160] clearly underestimates the low-frequency bend and even the tunneling barrier.[72] Thus, a PES should ideally be judged by its overall performance in comparison to as many different experiments as possible, rather than by results for a specific property. Equally important, accurate dynamical methods must be employed for judging fine details, since approximations can lead to error compensations generating a fortuitous deceptive agreement between experiment and theory. The latter did happen for the ground-state tunneling splitting[116] and perhaps also the K-rotational excitation of the out-of-plane bending mode[76] (see Section 5.4).

5.3. Hydrogen Bond Dissociation

The breaking and making of hydrogen bonds is at the heart of biochemical processes, condensation and evaporation phenomena, and other important processes. Hence it deserves particular attention in the simple prototype $(HF)_2$. With the accurate experimental determination of the dissociation energy[175,176] of $(HF)_2$, $D_0 = 1062 \pm 1$ cm^{-1} and the extension to mixed isotopomers,[48,76,177,178] useful benchmarks for high quality dimer PES have become available via DQMC and Eq. 6. These are matched in our recent SC-2.9 and SO-3 pair potentials,[72,87] and even

the less accurate SQSBDE PES has been of some help in the experimental assignments.[48,178] Our best prediction of the as yet unmeasured $(DF)_2$ dissociation energy would be 1175 cm^{-1}, with an estimated uncertainty of ±5 cm^{-1}.[72,87]

Despite obvious quantitative limitations, a one-dimensional picture of dissociation can have its merits. Such a one-dimensional picture should however include the zero-point energy of the remaining vibrational modes, i.e. it should be based on adiabatic channels.[76,113,132,179] As discussed in Section 4.2, the DQMC method lends itself very well to the construction of selected adiabatic channels,[76] and this principle has been adapted for other systems as well.[129,180] In the case of the dimer, adiabatic channels are also generally accessible from variational calculations.[107,108] Via such an adiabatic treatment, the F–F stretching fundamental has been successfully predicted near the experimental location of 125(5) cm^{-1},[76] which is also confirmed by extrapolation from near-infrared combination band spectroscopy.[46]

The manifold of adiabatic channels without HF stretch excitation determines the *thermal* dissociation kinetics of $(HF)_2$, which has not yet been studied experimentally in any detail.[8,181] Much more attention has been devoted to photochemical (pre) dissociation of the dimer ever since the first high-resolution HF stretching spectra[5] and a multitude of state-specific predissociation data have been collected since then.[16,43,44,46,47,53,57,59,155,176,177,182–187] It is found that predissociation in $(HF)_2$ is sensitive to rotational, tunneling, HF stretching, and hydrogen bond mode excitation, with lifetimes ranging from a few ps to more than 20 ns. Several simplified models[59,167,188–191] have been proposed, but none of them is able to explain all the data. In this situation, multidimensional golden rule[97] and time-dependent[98] predictions should prove very useful[99] when combined with sufficiently accurate PES.[72,87] Together with detailed photofragment distributions,[176] the predissociation lifetimes provide very sensitive tests of the accuracy of the PES beyond the regions of configuration space which are probed by the hydrogen bond fundamental vibrations. Preliminary results, based on the early SQSBDE surface,[76] are quite promising.[97]

5.4. Hydrogen Bond Libration

When a hydrogen bond is formed, the engaged hydrogen atom becomes constrained within the plane perpendicular to the bond. In principle, this gives rise to a degenerate pair of vibrational degrees of freedom, called librations. Due to a small departure of the hydrogen bond from linearity and due to the nonlinear arrangement of the second hydrogen in HF dimer, the degeneracy is lifted and one can distinguish an in-plane and an out-of-plane libration. The out-of-plane libration ν_6 was the first hydrogen bond mode to be detected and assigned experimentally[6] in $(HF)_2$ at rotational resolution, and the initial $K = 1$ assignment has been extended to $K = 2$[165] and tentatively also to $K = 3$,[76] the latter being based on approximate calculations without supporting rotational analysis of the spectrum. Here K is the quantum number for rotation parallel to the librational plane, i.e. around the F–F axis. Around

this axis, rotation is strongly quantized in HF dimer due to the absence of heavy off-axis atoms.[53,173] This also explains the strong K dependence of the tunneling splitting, since centrifugal forces push the equilibrium geometry towards the interconversion saddle point[53,173] (Figure 6). The in-plane libration ν_3 was the last hydrogen bond mode to be found experimentally, until today only in combination with an HF stretching mode.[47] For both librations, the $K = 0$ fundamental band origin remains unknown. The smooth behavior of the $K = 1, 2, 3$ levels of ν_6 suggested an extrapolated $K = 0$ band center of $\tilde{\nu}_6 \approx 380$ cm^{-1}.[76,106] This was apparently supported by *approximate* DQMC calculations (neglecting Coriolis couplings[76]) of the $K = 1, 2, 3$ levels for the SQSBDE surface in excellent agreement with experimental data.[76] On the same PES, *exact* DQMC calculations of $K = 0$ yield $\tilde{\nu}_6 = 378$ cm^{-1}.[76] However, variational calculations[97,107,112] reveal a complex Coriolis coupling situation for $K > 0$ with pronounced level shifts, while they confirm the rigorous DQMC prediction for $K = 0$. The coupling is actually so strong that it pushes the $K = 1$ level *below* the $K = 0$ level (see Figure 4), a remarkable and rarely found situation,[192] which had been discussed as a possibility for HF dimer spectra assignments before,[6,193] but without definitive conclusions. Hence, it turns out that inaccuracies in the SQSBDE surface[76] and the underlying ab initio data base[75] are compensated by neglect of Coriolis coupling in the excited K states, a notion which is supported by isotopomeric dissociation energies[48,177] and high-level ab initio predictions.[70,71] The new SC-2.9 and SO-3 PES, which are based on a much larger ab initio basis set than SQSBDE, predict a more anisotropic librational subspace. Now, a much higher ν_6 fundamental band center $\tilde{\nu}_6 \approx 420$ cm^{-1} is found to be compatible with the observed $K > 0$ states[17,72] as well as with combination band data.[47,72,107,108] The $K = 0,1$ level inversion persists and is thus seen to be a robust feature of the various $(HF)_2$ PES. In contrast, the $K = 1$ ν_6 tunneling splitting is found to be very sensitive to details of the PES, differing by a factor of 5 between SQSBDE and SC-2.9 and still by about 20% between the very similar SO-3 and SC-2.9 surfaces.[72,87,96] We note that a band near 380 cm^{-1}, which several plausible assignments have been proposed,[6,76] may involve the missing $K = 0$ level of ν_6 in a $\Delta K = -1$ transition from the vibrational ground state. This and the missing direct evidence for the ν_3 fundamental near 480 cm^{-1} suggest an experimental reinvestigation of the relevant far-infrared region, which is currently underway in our laboratory by improved FTIR-long path cell absorption techniques.

6. SPECTROSCOPY AND DYNAMICS OF THE HF TRIMER

Given a sufficiently complete characterization of the HF dimer spectroscopy and quantum dynamics, the trimer $(HF)_3$ offers the unique opportunity to extract and evaluate three-body contributions to hydrogen bonding.[8,68] Although the number of internal degrees of freedom is doubled relative to the dimer, the C_{3h} symmetry of this cluster should assist a rotationally resolved spectral analysis. Nevertheless,

relatively little is known experimentally about the gas-phase IR spectrum of $(HF)_3$ and its isotopomers. A comprehensive predissociation study with isotopic substitution[64] indicates that $(HF)_3$ can decay into three monomers as well as into a dimer and a monomer upon excitation of the HF stretching fundamental. From the isotopic substitution pattern, a cyclic structure with C_{3h} symmetry can be inferred, but rapid intramolecular vibrational redistribution (IVR) and predissociation on a 2–20 ps timescale preclude an accurate structure determination.[64] DQMC calculations on a full-dimensional PES including the three-body term[68] confirm that two predissociation channels are open to $(HF)_3$ after HF stretch excitation, with the three-monomer channel being almost closed for cold clusters, as generated in a supersonic beam. This changes with successive deuteration,[68] and *no* open predissociation channel is finally predicted for $(DF)_3$.[68] Again, the prediction is borderline, with the dimer + monomer channel being nearly open. However, subsequent improvements in the PES[72,89] confirm the prediction, whereas neglect of anharmonic zero-point contributions or neglect of three-body effects would reverse it.[68]

In order to test the cluster stability and structure predictions made by the PES, a high-resolution IR spectrum of the DF stretching fundamental of $(DF)_3$ was recorded.[31,45] It consists of a dense line pattern including Doppler limited lines, indicative of excitation below (or at best very slightly above) the lowest dissociation channel. From the coarse-grained spectral structure, the cluster symmetry, planarity, and rotational constants can be derived. These are in good agreement with the predictions on the three-body inclusive PES, if (and only if) multidimensional zero-point averaging is taken into account.[31,68,194] The resulting F–F distance is 257–260 pm, where the uncertainty is dominated by possible anharmonic Coriolis contributions to the effective rotational constants. This is significantly shorter than the corresponding estimate for HF dimer[8,72] of 273.5 ± 1 pm, in line with the important role of three-body contributions. In addition to providing a crucial test for the quality of the available three-body PES, the experimental spectra contain evidence for a rapid IVR process on a time scale of about 40 ps,[45] apparently involving essentially all available rovibrational states of a given J quantum number and therefore a multitude of states with up to nearly two hydrogen bonds broken. This is an interesting example of highly "statistical, global"[195] rovibrational dynamics near dissociation threshold, for which quantum-dynamical calculations remain to be performed.

Little is known experimentally about the low-frequency modes of $(HF)_3$. An IR double-resonance study provides evidence for two overtone states in the CO_2 laser range, which were tentatively assigned via reduced dimensionality calculations.[65] For the fundamentals themselves, approximate DQMC calculations were carried out on the older PES.[68] They suggest that the anharmonic band centers lie 15–25% below the corresponding harmonic frequencies, although this may change somewhat for the new SO-3 + HF3BG surface. Noteworthy is an inverse isotope effect for the F–F stretching vibration ν_{FF} in $(HF)_3$ and in $(DF)_3$ ($\tilde{\nu}_{FF}[(HF)_3] <$

($\nu_{FF}[(DF)_3]$), found in matrix spectra[196] and confirmed by calculations on the PES.[31,68] Harmonic predictions on the PES[8] are in good agreement with high-level ab initio benchmarks,[154] although both harmonic force fields may still be in error by several percent and experimental data would be highly desirable.

The experimental study of the trimer is complicated by the lack of substantial amounts of this cluster in the gas phase because its high ring strain leads to a relatively low stability compared to the tetramer and pentamer.[8,31,69] In fact, at and slightly above room temperature the rings are predicted to be broken up to open chains to a significant degree. This is not the case for the larger ring clusters, on which we will concentrate in the next section.

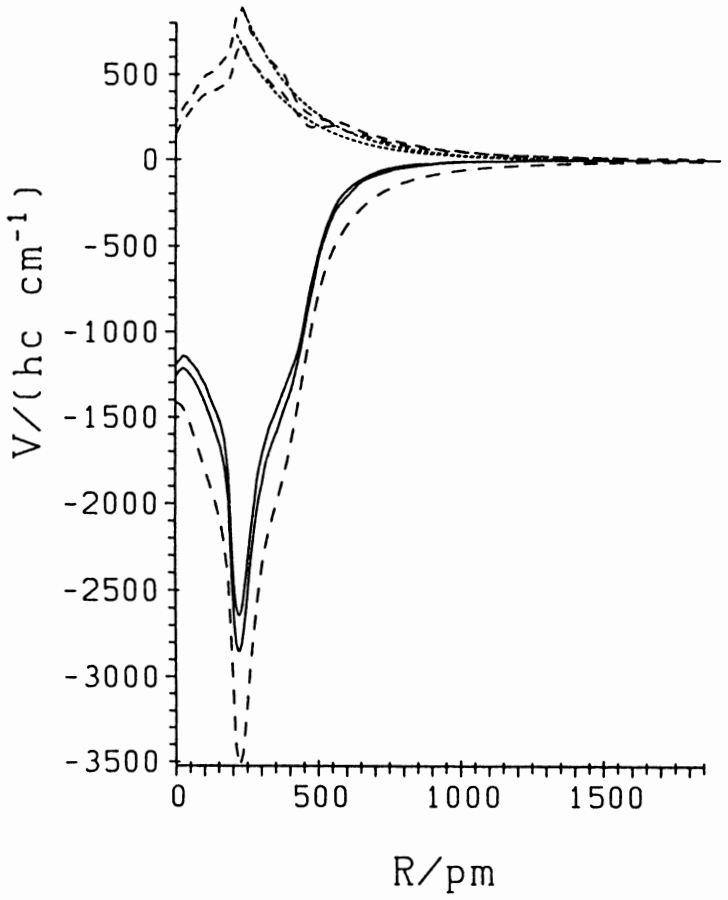

Figure 7. One-dimensional minimum energy path (dashed) and $(HF)_3$ (upper), (DF)3 (lower full curve) lowest adiabatic channels for dissociation into a dimer and a monomer, obtained from the SNB + HF3BL PES[68] via clamped coordinate DQMC. *R* is the distance between monomer and dimer centers of mass. All channels are referred to zero for infinite separation. Dashed lines with positive energies represent the zero-point energy along the path (upper: H; lower: D isotopomer) and the fine dashes represent an exponential fit[113] with $\alpha = 0.45$ Å (see also ref. 76).

Dissociation of the trimer may occur in two steps. For illustration, we show in Figure 7, the lowest adiabatic channel $V_Q(R)$ for fragmentation of the trimer $(HF)_3$ leading to $(HF)_2$ + HF as a function of center-of-mass separation R of the two fragments.[68] Also shown is the correspondingly steeper channel for $(DF)_3$, which explains the inverse isotope effect discussed above. These one-dimensional channels include the effective anharmonic zero-point motion of all but the reaction coordinate (R) modes. The inflection in the outgoing channels marks the breaking of one hydrogen bond to form a floppy chain, followed by a steeper increase of the energy when the second bond is broken. According to the analytical PES and DQMC calculations along this reaction path, there seems to be no electronic or zero-point energy barrier for the reverse formation of the trimer out of a dimer and a monomer. However, other reaction paths are conceivable for this complex and may involve such a barrier. We note that the recombination $(HF)_2 + HF \rightarrow (HF)_3$ is special in the reactant $(HF)_2$ having an open chain structure, into which HF can insert directly without breaking a hydrogen bond. The process is less simple for the larger clusters.

7. SPECTROSCOPY AND DYNAMICS OF HIGHER HF OLIGOMERS

It is now well established that larger oligomers $(HF)_{n\leq 6}$ have a planar or nearly planar ring structure.[8] HF ring clusters of larger size have been postulated for decades to account for the unusual properties of the HF vapor phase.[3,197–199] Without going into the historical details, we emphasize that the preeminent role of the hexamer in this context should be viewed more as that of a representative for a range of three to four important medium-sized clusters,[9] rather than as a singularly abundant species such as S_8 in elemental sulfur chemistry. We will not deal with thermodynamic vapor-phase data[198,200] which provide rigorous tests of the available PES, if both the data and the dynamical analysis are sufficiently accurate.[9,76] Rather, we concentrate on the size-specific spectroscopic evidence which has accumulated over the past years and which has given rise to some controversy, recently.[41,42,52,61,201–204]

7.1. Experimental HF Stretching Spectra as Assigned to Different Cluster Sizes $(HF)_n$

Forty years ago, recognizing the power of IR spectroscopy in elucidating the dynamics of HF clusters, Smith[15] recorded equilibrium spectra of HF vapor in a wide range of temperatures and pressures. While both the librational and the HF stretching region were studied, the latter is most conclusive in terms of cluster composition (Figure 8). Two strong, broad, overlapping bands were found considerably shifted to lower frequencies with respect to the free monomer transitions around 3961 cm^{-1}. From the pressure dependence of the IR absorption on the outer

wings of the bands (see Figure 8), Smith concluded that the band to lower wavenumbers is due to $(HF)_6$ and the one at higher wavenumbers due to $(HF)_4$. While Smith's early results could be experimentally confirmed by more recent FTIR-spectroscopy of HF vapor under equilibrium conditions at various temperatures in cells[16](Figure 8), questions arose concerning the *assignments* of the cluster spectra. In the light of more recent theoretical calculations of the energetical and spectral properties of these clusters,[67,68] based also on our dimer PES[76] complemented by a three-body term,[68] the most puzzling fact was the apparent absence of evidence for the intermediate pentamer, $(HF)_5$, while the existence of only one IR-active band per cluster can be easily explained by the C_{nh} symmetry.[41,67]

This provided the motivation for recording HF cluster FTIR spectra under supersonic jet conditions to reduce inhomogeneous broadening.[41] Earlier molecular beam spectra of HF clusters[49,62] had been too far away from the thermodynamical vapor-phase composition to be useful in this context. By choosing a wide range of expansion conditions (backing pressure, dilution in He, nozzle distance) it is possible to smoothly reduce spectral congestion without losing track of the thermal equilibrium spectra.[41] The jet spectra reveal an additional band, hidden underneath the inhomogeneous double-hump structure of the cell spectra (Figure 8). Upon cooling, all band maxima shift to lower wavenumber, thus allowing an

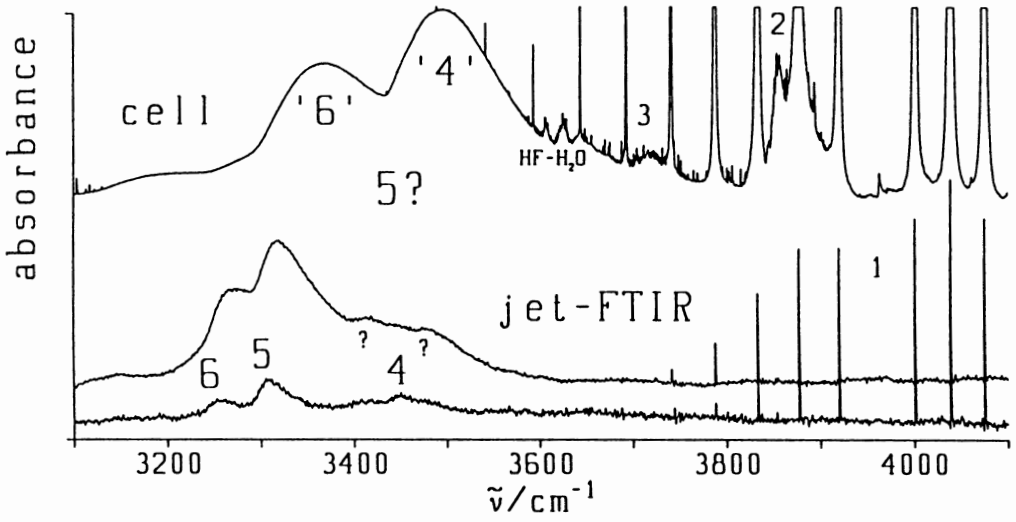

Figure 8. Comparison of cooled cell[15,16] and early He-seeded jet FTIR spectra[41] of HF. In the cell spectrum (T = 264 K) one can see rotational lines of HF (**1**), subbands of the dimer (**2**), a weak trimer absorption (**3**), HF–H_2O impurities and two broad bands ('**4**', '**6**'), assigned by Smith to the tetramer and hexamer of HF.[15] Two jet spectra[41] with expansion temperatures of ≈200 K (middle) and ≈150 K (lower trace) illustrate considerable thermal shifts of the large cluster bands and reveal an additional band (**5**), which we assign to the pentamer.[41]

approximate extrapolation to the 0 K homogeneous band structure. By adopting Smith's pressure-dependence results, by considering the dependence of the band intensities on expansion conditions, and by comparing to matrix isolation spectra[196,205] and harmonic ab initio frequency shift predictions relative to the monomer as a guidance, we tentatively proposed the cluster size assignment shown in Figure 8, namely a tetramer band near 3445 cm^{-1}, a pentamer band at 3300 cm^{-1}, and a hexamer band at 3245 cm^{-1}, all of them most likely HF stretching fundamentals.[41]

This assignment was later challenged[202] by a combined predissociation-scattering investigation based on the powerful "size-selective" technique of Buck and Meyer[206] with some modifications.[61] Through a combination of mass-spectroscopic detection with He beam scattering, the ambiguity due to cluster ion fragmentation in the mass spectrometer is minimized. Basically, a size assignment shifted by one monomer unit is proposed[61,202] as compared to ref. 41, i.e. the band originally assigned to $(HF)_5$ is claimed to be due to $(HF)_6$ etc. A $(HF)_4$ band near 3636 cm^{-1} can be unambiguously identified, whereas no band is found at 3445 cm^{-1} to be assigned[41] the tetramer. Slightly shifted from that position, near 3453 cm^{-1}, and in close vicinity of a power gap in the dissociating laser, a band is found and assigned to the pentamer based on its scattering angle dependence, which clearly differs from that of the 3636 cm^{-1} band. Building on this, the lower frequency predissociation bands, which agree in position with the FTIR spectra,[41] are assigned to the hexamer (3300 cm^{-1}) and heptamer (3245 cm^{-1}).

In contrast, our own FTIR reinvestigation of the spectra, resulting in much better signal-to-noise ratios through the use of the synchronously pulsed technique,[9,42,52] confirms our original assignment (Figure 9[41]). Furthermore, we suggest a plausible interpretation of the previously unassigned bands in terms of combination bands with a totally symmetric ring breathing vibration,[42,207,208] in excellent agreement with extensive theoretical calculations[42] and with additional support from deuteration experiments.[52]

In our view, the key problems of the $(HF)_n$ predissociation-scattering experiment[61,202] and our suggested explanations are the following:

1. The $(HF)_4$ band near 3636 cm^{-1} is most likely not due to a *fundamental* HF stretching transition. We suggest that it is a combination band,[42] such as the ones we find for $(HF)_5$ and $(HF)_6$, in excellent agreement with theoretical and far-infrared[9] evidence.
2. The "pentamer band" near 3453 cm^{-1} in the predissociation experiment falls in between the FTIR tetramer fundamental at 3445 cm^{-1} and the FTIR pentamer combination band near 3470 cm^{-1}. We suggest that it continues into the laser power gap and that it may in fact be largely identical to the FTIR combination band.
3. There is no band in the predissociation spectrum coinciding with the FTIR tetramer band at 3445 cm^{-1}. We suggest that the cold tetramer gives a negligible predissociation signal because it is probably slightly below dissociation threshold after excitation near 3445 cm^{-1} (in analogy to the $(DF)_3$ case[31,45,68]),[17,41,42] as

illustrated in Fig. 10 below. Collision with He atoms for the purpose of size selection may induce fragmentation of the highly vibrationally excited clusters, but the resulting angular scattering distribution for successful fragmentation events will lack contributions at maximum angle due to the inelastic nature of the dissociative collision.[42] Thus, the tetramer may appear to have a larger kinematic mass. This is what one finds experimentally—an angular distribution between that of a tetramer and that of a pentamer.

4. The size assignments for the larger clusters ($n > 4$) in the predissociation-scattering experiment[61,202] essentially build on the assignment of the 3453 cm^{-1} band and may have to be revised accordingly.

We propose to repeat the scattering experiment with a warmer expansion (e.g. in He[201]) and to close the laser power gap.[209] The resulting spectra should be able to test our tentative interpretation, which appears to be the only one which is able to explain all available data. Alternative explanation attempts based on branched structures[203] or based on a fundamental HF stretch assignment of the 3636 cm^{-1} band[61] cannot explain the available experimental evidence[4,52] nor are they compatible with reliable theoretical results.[9,42,68]

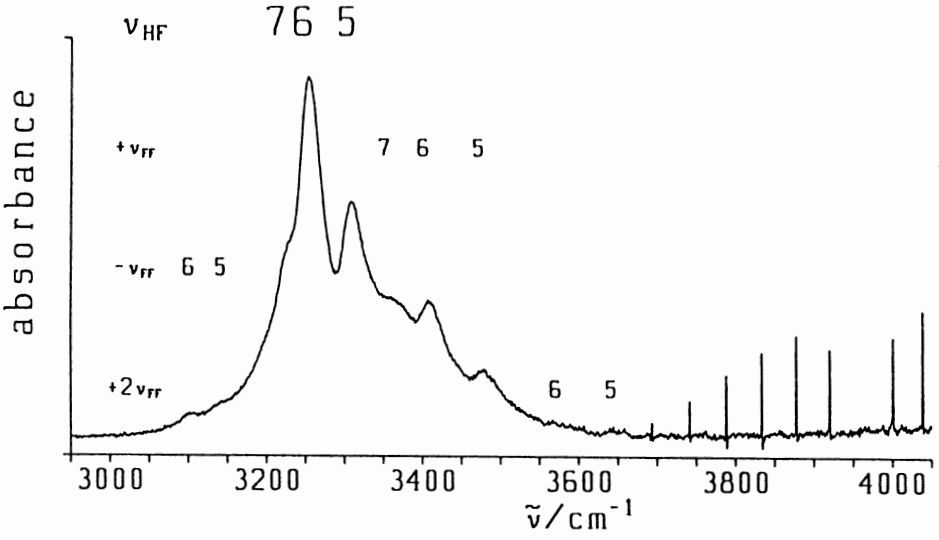

Figure 9. Synchronously pulsed jet FTIR spectrum[52] of HF diluted in He under conditions where $(HF)_n$ with $n = 5, 6, 7$ dominate the structured part of the cluster absorption. Compare also to Figure 8. In addition to fundamental HF stretching modes (ν_{HF}), combination ($+\nu_{FF}$, possibly $+2\nu_{FF}$) and difference bands ($-\nu_{FF}$), presumably with the totally symmetric FF stretching band,[9,42,52] can be seen. There is no need to invoke other than simple ring structures for the structured absorptions in the spectrum, while the broad background may be partly due to isomers[41,42,203] or larger clusters.[41]

While the only IR active HF stretching vibration in the planar cyclic HF clusters is the lowest degenerate (E) mode,[41,67] Raman spectroscopy can be used to detect the totally symmetric (A) HF stretching mode, which is part of the reaction coordinate for simultaneous exchange of all hydrogen atoms between adjacent fluorine atoms (see Section 7.5 and Eq. 8 below). Supersonic jet Raman spectra for HF clusters are not available, but the experimental difference between the IR active E and the Raman active A band maxima is $\approx 160\ cm^{-1}$ at room temperature.[15,37] This is consistent with theoretical predictions at harmonic level[42,69] in view of the large thermal and anharmonic effects.[41]

7.2. Stretching Frequency Shift Predictions

The controversial assignments discussed in the preceding section demonstrate the importance of reliable frequency predictions for the correct assignment of IR spectra of hydrogen bonded clusters.[41,42,52] The wavenumber shift $\Delta\tilde{\nu} = \tilde{\nu}_{HF}(HF) - \tilde{\nu}_{HF}((HF)_n)$ of the HF stretching vibration relative to the isolated HF molecule is most useful, because it depends strongly on cluster size. This shift is typically to lower wavenumbers for hydrogen bonds. $\Delta\tilde{\nu}$ as defined is thus positive. Three levels of treatment may be distinguished:

1. The harmonic approximation ($\Delta\omega$), which considers the local curvature at the cluster minimum and compares it to that of the free monomer. It is most popular in ab initio investigations because it can be obtained at relatively little extra cost and because it is apparently quite successful.[69,75,154]

2. A combined anharmonic treatment of the high frequency HF stretching degrees of freedom, while the intermolecular coordinates remain clamped to their minimum energy values. This approximation is sometimes used for one or two high-frequency modes,[210] whereas it becomes more demanding for a larger number of coupled anharmonic oscillators[211] such as in $(HF)_n$ with $n \geq 3$.[42] For these, we find that the anharmonic diagonal corrections can be quite large, increasing the shifts by 15 to 35%.[42]

3. Zero-point energy along the low-frequency hydrogen bond modes, in particular along the librational coordinates, weakens the effective interaction between the monomers. This indirect mode coupling is neglected in the harmonic approximation. Some qualitative aspects can be captured by a modification of the cluster geometry at which the harmonic approximation is applied.[212] More rigorously, the zero-point motion can be included adiabatically via DQMC bath treatments or by full-dimensional variational calculations.[72,94,107] The effect for HF clusters is to reduce the wavenumber shifts by about 10 to 30%, thus approximately *compensating* for the diagonal anharmonicity effect discussed in 2 above.

In combination with systematic basis set and correlation errors,[69,72] the effects mentioned under 2 and 3 explain why simple harmonic treatments according to 1 are often surprisingly successful in predicting fully anharmonic experimental

frequency shifts, in particular once they are scaled or designed to reproduce experiment for a given cluster size. One should not interpret this success of the harmonic approximation as evidence for harmonic behavior in hydrogen bonding.

7.3. Intracluster Vibrational Redistribution

After HF stretching excitation, most HF clusters have two pathways available for the redistribution of the deposited energy[16] (see ref. 36, 213 for conceptual aspects). The energy may flow within the HF stretching manifold and into bound hydrogen bond modes (intramolecular vibrational redistribution, IVR) or it may lead to dissociation of the cluster, i.e. it may partially flow into fragment translation and rotation (predissociation, PD). In the HF dimer, predissociation in $N = 1$ or $N = 2$ stretching manifold cannot be described as a *sequential* process of IVR followed by dissociation, because the density of quasibound rovibrational levels is too low.[16] It is thus "direct" or semidirect with off resonance intermediates.[214] This gives rise to highly nonstatistical rates, as discussed above (Section 5.3). In the larger, more strongly bound and more strongly coupled clusters, direct predissociatilon after HF stretching excitation is also an option in many cases, at least energetically (see Figures 10, 11). However, there are indications[45,52,64] that in these systems dissociation may typically be preceded by fast and extensive IVR processes, the dissociation process would thus be sequential. It is conceivable but by no means certain that the second step of dissociation can be described by statistical theories.[215]

From the widths of the $(HF)_n$ and $(DF)_n$ absorptions with $n = 5$ to 7 recorded in a supersonic jet[42,52] (Figure 9) one can derive 0.3 ps as a lower bound for τ_{IVR} after HF (DF) stretching excitation. This is most likely a speedup of IVR relative to $(HF)_3$ (2–20 ps)[64] and $(DF)_3$ (40 ps).[45] While there may be residual contributions to the widths such as inhomogeneous structure and direct predissociation (in the case of $(HF)_n$, see Figure 10), there is evidence that these are not dominant,[52] although vibrationally inhomogeneous structure is difficult to exclude in the jet expansions. Matrix isolation spectra at low temperatures[205] exhibit bandwidths comparable to those in the supersonic jet, but here, the possibility of inhomogeneous broadening due to the matrix environment has to be considered. A decay time of 0.3 ps can be compared[216] in magnitude to macroscopic sound propagation across a single hydrogen bond distance of 150 pm in liquid HF, which is among the liquids with a particularly low speed of sound.[217] However, vibrational energy migration by sound is not identical to IVR. Further experimental and theoretical investigations will be required before a definitive confirmation and explanation for this apparently very fast IVR process can be given. The great increase in the rate of IVR in $(HF)_{n\geq4}$ compared to $(HF)_3$ can be associated with a systematic increase of the highest low-frequency modes in the larger clusters, which breaks the adiabatic separation of high- and low-frequency modes.

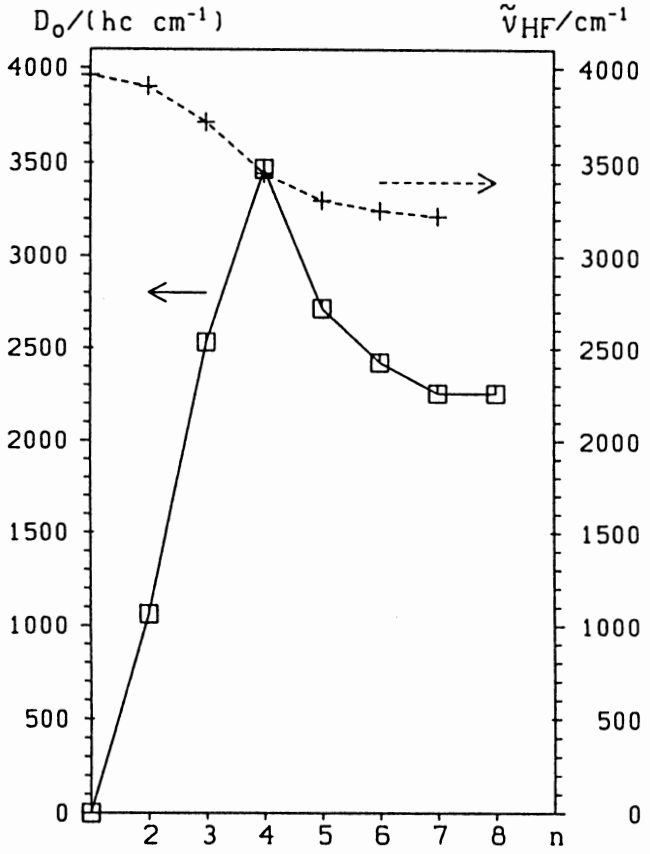

Figure 10. Comparison of best estimates for the stepwise dissociation energy ΔD_0 (left scale, □) according to $(HF)_n \rightleftharpoons (HF)_{n-1} + HF$ with the IR active fundamental excitation wavenumber $\tilde{\nu}_{HF}$ (right scale, +; for $n = 2$ the average of the two IR active bands is chosen, for $n > 5$ the strongest band is shown) according to current assignment[41,42,53,64] as a function of cluster size n. Where D_0/hc is above $\tilde{\nu}_{HF}$, the cold cluster is stable with respect to single-photon excitation. This is probably the case for $(HF)_4$.

7.4. Cluster Isomerization

With increasing cluster size, the number of possible $(HF)_n$ isomers and their interconversion pathways grows quickly. For HF trimer, these are briefly summarized in Figure 6 of ref. 9. Starting with the tetramer, the number of isomers consisting of smaller rings with attached side chains grows quickly with size.[42,68,203] They may play a dynamical role as intermediates in cluster growth[9] and hydrogen bond isomerization processes,[17] but thermodynamically they are not competitive with simple ring structures up to at least the hexamer. For even larger cluster sizes, sandwich structures of two and more ring clusters become competitive.[9,68] Our strategy to characterize cluster isomerism is to combine Monte Carlo searches with deterministic minimizations on the inexpensive analytical PES, with subsequent

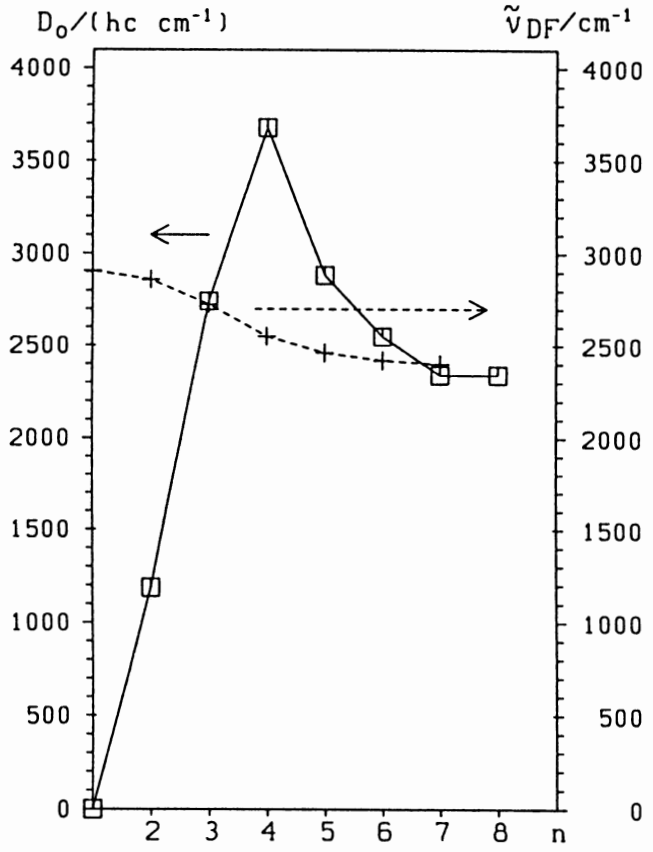

Figure 11. Comparison of best estimates for the stepwise dissociation energy ΔD_0 (left scale, □)) according to $(DF)_n \rightleftharpoons (DF)_{n-1}$ + DF with the IR active fundamental excitation wavenumber $\tilde{\nu}_{DF}$ (right scale, +; for $n = 2$ the average of the two IR active bands is chosen, for $n > 5$ the strongest band is shown) according to current assignment[45,52,53] as a function of cluster size n. Where D_0/hc is above $\tilde{\nu}_{DF}$, the cold cluster is stable with respect to single-photon excitation. This is the case for $(DF)_n$ with $3 \leq n \leq 6$, possibly also for larger clusters.

verification via ab initio minimizations. In between such a mapping of local minima and a full dynamical investigation of the interconversion processes, there is a wide range of topological studies of the multidimensional PES[218,219] and order of magnitude estimates for interconversion tunneling splittings[220] which can be carried out.

7.5. Concerted Hydrogen Exchange

The HF cluster dynamics discussed so far retains the integrity of the HF molecules, and this fact is exploited in the PES representation.[8] However, there is early NMR-spectroscopic evidence that the monomer integrity is broken in the gas phase on a nano- to microsecond timescale[17–19,69] via reactive processes of the type as shown by Eq. (8):

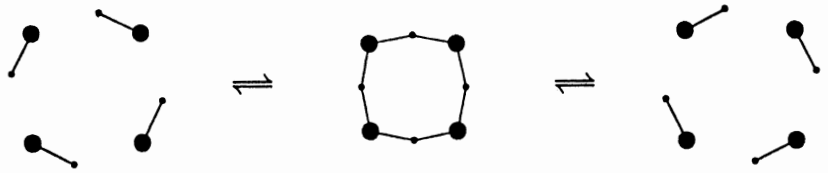

(8)

Reliable ab initio predictions of the barriers for such concerted hydrogen exchange processes are quite demanding, as electron correlation and basis set requirements are very high.[69] The best available data hint at a zero-point energy corrected barrier of 40 ± 10 kJ mol^{-1} for both the tetramer and the pentamer,[17] with smaller clusters having substantially higher barriers.[17,69] This barrier size is consistent with experimental rate data,[18] even without tunneling corrections, which may be quite significant in these systems.[221,222] More detailed kinetic predictions will have to wait for analytical PES[8,223] or new interpolation techniques[224–227] which can describe the exchange process, for appropriate reduced dimensionality treatments,[69] or for accurate on-the-fly dynamical evaluations.[221] Experimentally, there is so far no evidence for the exchange process from infrared spectroscopy,[52] although high-resolution far-infrared spectroscopy may be able to resolve the associated splittings.[14,24] On the NMR side, a reinvestigation of the gas-phase dynamics at low temperatures and pressures might be rewarding.[17]

In the context of the preceding section, it should be emphasized that HF stretching excitation in HF oligomers is close to the threshold for hydrogen exchange for $n \geq 4$. This can be seen in relation to the rapid IVR observed in these bands,[52] although many dynamical aspects have to be considered.

8. HYDROGEN FLUORIDE NANOCLUSTER DYNAMICS

The $(HF)_n$ clusters discussed so far may be considered "natural," as they constitute a substantial fraction of the vapor phase at thermodynamic equilibrium,[9,41] under typical cell conditions.[16] Supersonic jet expansions offer the opportunity to generate even larger clusters by increasing stagnation pressure. The HF stretching spectra observed under these expansion conditions change qualitatively, as shown in Figure 12. The low-pressure expansion is dominated by medium-sized ring clusters, as discussed in Section 7.1. At higher pressures, two strong, broad bands emerge at lower and higher wavenumbers. These bands have no correspondence in the gas-phase spectra of HF nor do they coincide with the broad, unstructured band of liquid HF at room temperature.[228] However, they correspond quite well to the symmetric and antisymmetric HF stretching bands in solid HF,[229] both in band position and in relative intensity (Figure 12). Only the lower frequency band is slightly shifted to higher wavenumber in the cluster spectra. It thus seems that these clusters have a solid-like structure.

Solid HF is known to consist of infinite hydrogen-bonded zig-zag chains.[230] Interaction between the chains is weak and their relative dipole orientation has been controversial but is now known to be parallel,[231] at least for DF. Thus, solid HF may

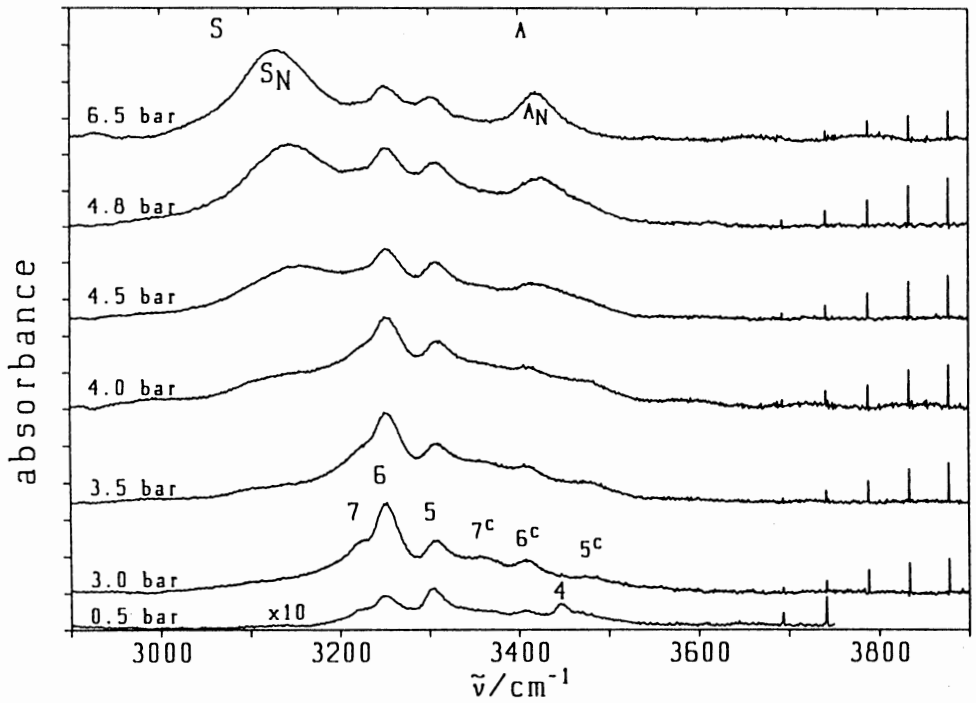

Figure 12. Jet FTIR spectra of HF expansions in He, with backing pressure and dilution increasing from the bottom to the top. The ring cluster bands visible at low pressures (marked with a number for fundamentals and with a superscript *c* for combination bands according to our assignment) vanish in favor of two broad bands (S_N, A_N) which correspond closely to solid state absorptions (indicated with S, A). For details see ref. 52.

be the chemically simplest ferroelectric.[232] The IR spectrum is dominated by the strongly coupled hydrogen bonds within the chains, which give rise to an unusually large splitting between the fully symmetric (in phase) and pairwise antisymmetric (antiphase) HF stretching fundamentals.[229] The slow convergence of these fundamentals and in particular of the low-frequency component with chain length has been studied in detail,[233] and we give a further illustration of this in Figure 13. The spectrum of a single HF molecule embedded in a chain of DF molecules shows a less pronounced chain length dependence (Figure 13), in agreement with experiment.[52]

It is tempting to interpret the experimental shift of the cluster band (S_N) relative to the solid (S, Figure 13) as a measure of chain length, but there could be other reasons such as crystalline disorder. From the absence of pronounced scattering contributions to the spectrum, one may however conclude that the cluster size is clearly below 1 μm. On the other hand, a subnanometer size should give rise to larger deviations from the solid spectra due to surface effect,[234] hence the designation "nano(meter)crystalline" appears to be appropriate.[52]

The nanocluster *phase*[235] deserves further attention. During aggregation, these clusters are most likely liquid because of the release of condensation energy. Due

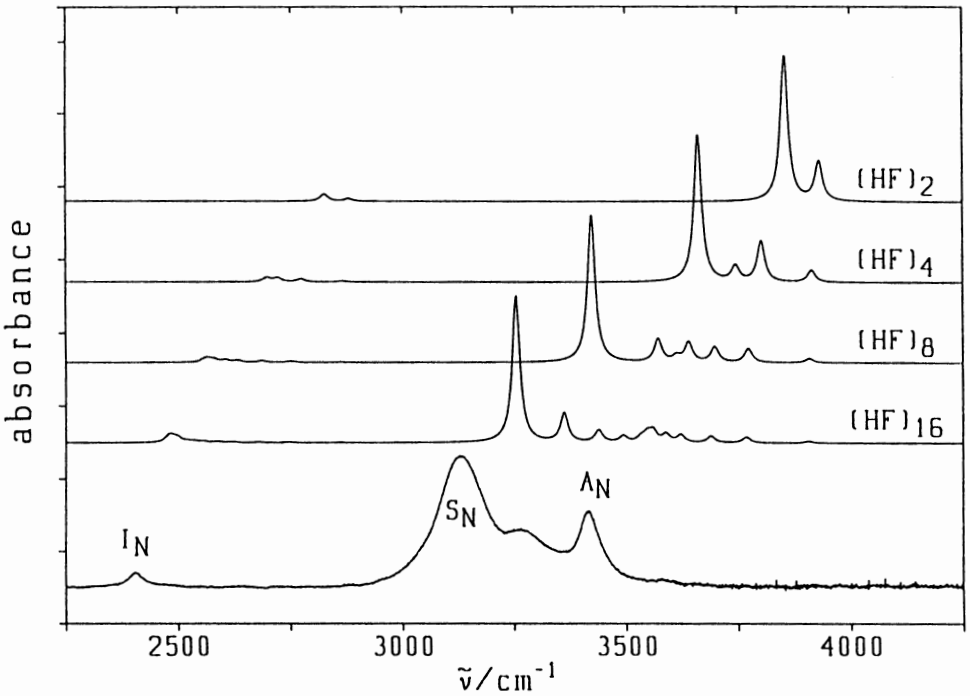

Figure 13. Simulation of $(HF)_n$ zig-zag chain spectra (n = 2, 4, 8, 16) with 9% DF impurity statistically distributed over the chain. Harmonic wavenumber shifts relative to free HF and DF from hybrid density functional (B3LYP 6-31+G*) force field calculations are scaled by 0.75 for HF stretches and by 0.80 for DF stretches before convoluting the transitions with a 20 cm^{-1} Lorentzian band profile. The scaling factors approximately take into account the overestimation of frequency shifts at B3LYP 6-31+G* level[69] and anharmonic contributions.[42] The spectral changes from n = 2 to n = 16 illustrate the slow convergence of the stretching frequencies with chain length. It is seen that the experimental spectrum (bottom trace, 4% HF and an impurity of DF in Ar, expanded at a backing pressure of 7.5 bar[52]) is probably due to a distribution of clusters containing significantly longer chains. The symmetric stretch (S_N) is clearly seen in all simulated spectra, whereas the antisymmetric stretch (A_N) only starts to be visible as a cluster of transitions in the n = 16 chain due to the lack of appropriate boundary conditions.[233] The isotopically isolated DF stretch vibration (I_N) converges more rapidly with cluster size.

to evaporative cooling, they may ultimately freeze, and this homonucleation kinetics has been modeled recently.[236] Details may certainly depend on expansion conditions and nozzle geometry, but a large number of experimental cluster phases determined by electron diffraction in Laval expansions can be modeled with remarkable success by a simple expression, which merely depends on the liquid range (interval between normal melting (T_m) and boiling (T_b) temperatures) of the compound and its melting entropy (ΔS_m) according to[237]

$$R_c = \frac{T_b - T_m}{T_b} + 0.007\left(\frac{\Delta S_m}{R}\right)^2 \tag{9}$$

R_c values above 0.32 correlate with liquid-like clusters, whereas compounds with R_c values below 0.3 are found to be solid. According to this expression, HF ($R_c \approx$ 0.39) should clearly form liquid clusters, and our evidence for solid clusters seems to provide the first exception to the nucleation model. This may be due to the unusual evaporation properties of HF[9] or it may simply reflect differences in expansion conditions. Clearly, this finding requires further systematic investigation. There may be important kinetic effects[16] in HF condensation, beyond the simple, quasithermodynamic model of ref. 237. Very recent results for water,[50] which falls in between the liquid and solid regimes of Bartell's rule, seem to indicate both liquid and solid nanoclusters. Supersonic jet generation of nanometer size material is an interesting alternative to methods using a cold buffer gas,[238–241] as it enables the study of short-time behavior under collision-free conditions in these exciting new states of matter.

9. CONCLUSIONS AND OUTLOOK

We have illustrated several facets of hydrogen bond dynamics in this review by covering cluster sizes from two to many hundreds or thousands of monomer units. We have considered fundamental processes such as state-specific tunneling and predissociation in $(HF)_2$, ring opening in the trimer, vibrational frequency shifts, hydrogen transfer and energy redistribution in the oligomers, and the phase dynamics of nanocrystalline clusters, thus revealing the prototypical role of hydrogen fluoride in this field. Some of the dynamical processes are summarized in Figure 14 as a function of cluster size and characteristic timescale. The latter is obtained from spectroscopic analysis leading to time-dependent molecular quantum dynamics[36,249] and theoretical predictions, whereas time domain experiments[216,242–244] are not yet available for infrared clusters. Several dynamical effects remain to be modeled in quantitative detail and the infrared spectra are not yet complete, but important progress is foreseeable in the near future. The recent development of a HF pair dipole surface,[87] which goes beyond simple induction models,[245] should provide useful infrared intensity information and other couplings of the HF dimer dynamics to electric fields[246] and laser radiation.[35,36,249] Still, important questions related to the hydrogen bond kinetics, thermally averaged or state specific, have to be answered before a truly comprehensive understanding of hydrogen bonding in $(HF)_n$ and its isotopomers can be claimed. Future work will concentrate on both experimental and theoretical approaches to quantitative kinetic data along these lines, deriving rate constants and quantum wavepacket motion for the underlying processes in hydrogen bonded clusters.

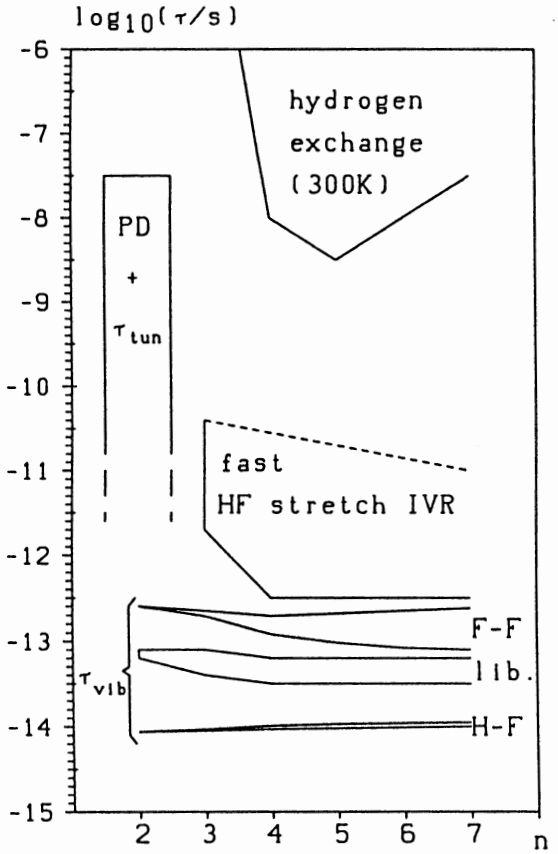

Figure 14. Schematic time scale diagram for typical dynamical processes in HF clusters as a function of cluster size *n* from femto- to microseconds. The vibrational periods (τ_{vib}) for F–F stretching, librational and H-F stretching modes remain separated from each other for all cluster sizes.[67–69] In the dimer, *observed* stationary state hydrogen bond exchange tunneling periods (τ_{tun}) and metastable state predissociation lifetimes (PD) (see Section 5) accidentally cover the same range,[16,53] but both can be much shorter for states which have not (yet) been observed or not yet analyzed. For larger clusters, intracluster vibrational relaxation (IVR) after HF stretching excitation probably becomes faster than direct predissociation.[45,52,64] Concerted exchange of hydrogen atoms between adjacent fluorine atoms in medium sized HF ring clusters is predicted to occur on a ns to μs time scale at room temperature.[17,221,222] In all cases, the indicated boundaries are only approximate.

ACKNOWLEDGMENTS

This work has profited from contributions by and discussions with a large number of people, most of whom can be found in the list of references. In particular, we should mention K. Al-Shamery (née von Puttkamer), Z. Bačić, L. Bartell, U. Buck, P. R. Bunker, E. U. Franck, R. B. Gerber, T.-K. Ha, Y. He, F. Huisken, A. Karpfen, W. Klopper, M. Lewerenz, K. Liedl, D. Luckhaus, C. Maerker, R. Marquardt, R. Meyer, R. E. Miller, H. Müller, D. Nesbitt, M.

Parrinello, K. Peterson, K. von Puttkamer, H. F. Schaefer III, P. von Ragué Schleyer, U. Schmitt, R. Signorell, J. Stohner, D. Truhlar, G. Tschumper, and J. Zhang. Our research is supported by the Schweizerischer Nationalfonds. We gratefully acknowledge generous allocations of computing resources by the Competence Centre of Computational Chemistry (C^4 project) in Zürich, and the Centro Svizzero di Calcolo Scientifico (CSCS/SCSC) in Manno, Switzerland.

REFERENCES

1. Hirschfelder, J. O.; Curtiss, C. F.; Bird, R. B. *Molecular Theory of Gases and Liquids*; Wiley: New York, 1954.
2. Pimentel, G. C.; McClellan, A. L. *The Hydrogen Bond*; Freeman, 1960.
3. Pauling, L. *The Nature of the Chemical Bond*, 2nd edn.; University Press: Oxford, 1940.
4. Dyke, T. R.; Howard, B. J.; Klemperer, W. *J. Chem. Phys.* **1972**, *56*, 2442–2454.
5. Pine, A. S.; Lafferty, W. J. *J. Chem. Phys.* **1983**, *78*, 2154–2162.
6. Puttkamer, K. v.; Quack, M. *Mol. Phys.* **1987**, *62*, 1047–1064.
7. Quack, M.; Suhm, M. A. *Chem. Phys. Lett.* **1990**, *171*, 517–524.
8. Quack, M.; Suhm, M. A. In *Conceptual Perspectives in Quantum Chemistry*; Calais, J.-L., Kryachko, E. S., Eds.; Conceptual Trends in Quantum Chemistry, Vol. III; Kluwer: Dordrecht, 1997, pp 417–465.
9. Suhm, M. A. *Ber. Bunsenges. Phys. Chem.* **1995**, *99*, 1159–1167.
10. Sievert, R.; Cadez, I.; Van Doren, J.; Castleman, Jr., A. W. *J. Phys. Chem.* **1984**, *88*, 4502–4505.
11. Simons, J. H. In *Fluorine Chemistry*; Simons, J. H., Ed.; Academic Press: 1950, Chapter 6, pp 225–259.
12. Badger, R. M.; Bauer, S. H. *J. Chem. Phys.* **1937**, *5*, 839–851.
13. Kappes, M.; Leutwyler, S. In *Atomic and Molecular Beam Methods*; Scoles, G., Ed.; Oxford University Press, 1988, Chapter 15, pp 380–415.
14. Quack, M. *Ann. Rev. Phys. Chem.* **1990**, *41*, 839–874.
15. Smith, D. F. *J. Chem. Phys.* **1958**, *28*, 1040–1056.
16. Puttkamer, K. v.; Quack, M. *Chem. Phys.* **1989**, *139*, 31–53.
17. Klopper, W.; Quack, M.; Suhm, M. A. *Mol. Phys.* **1998**, *94*, 105–119.
18. Mackor, E. L.; MacLean, C.; Hilbers, C. W. *Recl. Trav. Chim.* **1968**, *87*, 655–672.
19. Hindermann, D. K.; Cornwell, C. D. *J. Chem. Phys.* **1968**, *48*, 2017–2024.
20. Whaley, K. B. *Int. Rev. Phys. Chem.* **1994**, *13*, 41–84.
21. Truhlar, D. G. In *Proceedings of the NATO Workshop on the Dynamics of Polyatomic van der Waals Complexes, NATO Ser. B 227*, 1990, pp 159–185.
22. Buckingham, A. D.; Fan-Chen, L. *Int. Rev. Phys. Chem.* **1981**, *1*, 253–269.
23. Nesbitt, D. J. *Chem. Rev.* **1988**, *88*, 843–870.
24. Saykally, R. J.; Blake, G. A. *Science* **1993**, *259*, 1570–1575.
25. Chałasiński, G.; Szczęśniak, M. M. *Chem. Rev.* **1994**, *94*, 1723–1765.
26. Elrod, M. J.; Saykally, R. J. *Chem. Rev.* **1994**, *94*, 1975–1997.
27. Leopold, K. R.; Fraser, G. T.; Novick, S. E.; Klemperer, W. *Chem. Rev.* **1994**, *94*, 1807–1827.
28. Nesbitt, D. J. *Ann. Rev. Phys. Chem.* **1994**, *45*, 367–399.
29. Nesbitt, D. J. *Faraday Discuss.* **1994**, *97*, 1–18.
30. Klemperer, W. *Ann. Rev. Phys. Chem.* **1995**, *46*, 1–26.
31. Suhm, M. A.; Nesbitt, D. *Chem. Soc. Rev.* **1995**, *24*, 45–54.
32. Bačic, Z.; Miller, R. E. *J. Phys. Chem.* **1996**, *100*, 12945–12959.
33. Karpfen, A. In *Molecular Interactions—From van der Waals to Strongly Bound Complexes*; Scheiner, S., Ed., Wiley: New York, 1997, pp 265–296.

34. Robinson, J. M.; Pearson, D. J.; Copeland, R. A.; Crim, F. F. *J. Chem. Phys.* **1985**, *82*, 780–788.
35. Quack, M. In Broeckhove, J., Lathouwers, L. (Eds.). *Time Dependent Quantum Molecular Dynamics: Experiment and Theory. Proceedings of NATO ARW 019/92. NATO ASI Series Vol. 299*; Plenum Press: New York, 1992, pp 293–310.
36. Quack, M., Chapter 27 in Manz, J., Woeste, L. (Eds.) *Femtosecond Chemistry, Proc. Berlin Conf. Femtosecond Chemistry, Berlin, March 1993*; Verlag Chemie: Weinheim, 1995, pp 781–818.
37. LeDuff, Y.; Holzer, W. J. *Chem. Phys.* **1974**, *60*, 2175–2178.
38. Bürgi, T.; Droz, T.; Leutwyler, S. *Chem. Phys. Lett.* **1995**, *246*, 291–299.
39. Lafferty, W. J.; Suenram, R. D.; Lovas, F. J. *J. Mol. Spectrosc.* **1987**, *123*, 434–452.
40. Belov, S. P.; Karyakin, E. N.; Kozin, I. N.; Krupnov, A. F.; Polyansky, O. L.; Tretyakov, M. Y.; Zobov, N. F.; Suenram, R. D.; Lafferty, W. J. *J. Mol. Spectrosc.* **1990**, *141*, 204–222.
41. Quack, M.; Schmitt, U.; Suhm, M. A. *Chem. Phys. Lett.* **1993**, *208*, 446–452.
42. Luckhaus, D.; Quack, M.; Schmitt, U.; Suhm, M. A. *Ber. Bunsenges. Phys. Chem.* **1995**, *99*, 457–468.
43. Signorell, R.; He, Y.; Müller, H. B.; Quack, M.; Suhm, M. A. In Maier, J. P., Quack, M. (Eds.). *Proceedings of the 10th International Symposium on Atomic, Molecular, Cluster, Ion, and Surface Physics*; Vdf Publishers: Zürich, 1996, pp. 256–259.
44. Suhm, M. A.; Farrell, Jr., J. T.; McIlroy, A.; Nesbitt, D. J. *J. Chem. Phys.* **1992**, *97*, 5341–5354.
45. Suhm, M. A.; Farrell, Jr., J. T.; Ashworth, S.; Nesbitt, D. J. *J. Chem. Phys.* **1993**, *98*, 5985–5989.
46. Anderson, D. T.; Davis, S.; Nesbitt, D. J. *J. Chem. Phys.* **1996**, *104*, 6225–6243.
47. Anderson, D. T.; Davis, S.; Nesbitt, D. J. *J. Chem. Phys.* **1996**, *105*, 4488–4503.
48. Bemish, R. J.; Wu, M.; Miller, R. E. *Faraday Discuss.* **1994**, *97*, 57–68.
49. Sun, H.; Watts, R. O.; Buck, U. *J. Chem. Phys.* **1992**, *96*, 1810–1821.
50. Paul, J. B.; Collier, C. P.; Saykally, R. J.; Scherer, J. J.; O'Keefe, A. *J. Phys. Chem. A* **1997**, *101*, 5211–5214.
51. Anderson, D. T.; Davis, S.; Zwier, T. S.; Nesbitt, D. J. *Chem. Phys. Lett.* **1996**, *258*, 207–212.
52. Quack, M.; Schmitt, U.; Suhm, M. A. *Chem. Phys. Lett.* **1997**, *269*, 29–38.
53. Pine, A. S.; Lafferty, W. J.; Howard, B. J. *J. Chem. Phys.* **1984**, *81*, 2939–2950.
54. Amrein, A.; Quack, M.; Schmitt, U. *Z. Phys. Chem. N. F.* **1987**, *154*, 59–72.
55. Amrein, A.; Quack, M.; Schmitt, U. *J. Phys. Chem.* **1988**, *92*, 5455–5466.
56. Hartz, C. L.; Wofford, B. A.; McIntosh, A. L.; Meads, R. F.; Lucchese, R. R.; Bevan, J. W. *Ber. Bunsenges. Phys. Chem.* **1995**, *99*, 447–456.
57. Chang, H.-C.; Klemperer, W. *J. Chem. Phys.* **1994**, *100*, 1–14.
58. Gough, T. E.; Miller, R. E.; Scoles, G. *Appl. Phys. Lett.* **1977**, *30*, 338–340.
59. Pine, A. S.; Fraser, G. T. *J. Chem. Phys.* **1988**, *89*, 6636–6643.
60. Buck, U. *Ber. Bunsenges. Phys. Chem.* **1992**, *96*, 1275–1284.
61. Huisken, F.; Kaloudis, M.; Kulcke, A.; Laush, C.; Lisy, J. M. *J. Chem. Phys.* **1995**, *103*, 5366–5377.
62. Lisy, J. M.; Tramer, A.; Vernon, M. F.; Lee, Y. T. *J. Chem. Phys.* **1981**, *75*, 4733–4734.
63. Dayton, D. C.; Miller, R. E. *Chem. Phys. Lett.* **1988**, *143*, 181–185.
64. Michael, D. W.; Lisy, J. M. *J. Chem. Phys.* **1986**, *85*, 2528–2537.
65. Kolenbrander, K. D.; Dykstra, C. E.; Lisy, J. M. *J. Chem. Phys.* **1988**, *88*, 5995–6012.
66. Laush, C.; Lisy, J. M. *J. Chem. Phys.* **1994**, *101*, 7480–7487.
67. Karpfen, A. *Int. J. Quantum Chem. (Quant. Chem. Symp.)* **1990**, *24*, 129–140.
68. Quack, M.; Stohner, J.; Suhm, M. A. *J. Mol. Struct.* **1993**, *294*, 33–36. To be published.
69. Maerker, C.; von Ragué Schleyer, P.; Liedl, K. R.; Ha, T.-K.; Quack, M.; Suhm, M. A. *J. Comp. Chem.* **1997**, *18*, 1695–1719.
70. Peterson, K. A.; Dunning, Jr., T. H. *J. Chem. Phys.* **1995**, *102*, 2032–2041.

71. Collins, C. L.; Morihashi, K.; Yamaguchi, Y.; Schaefer III, H. F. *J. Chem. Phys.* **1995**, *103*, 6051–6056.
72. Klopper, W.; Quack, M.; Suhm, M. A. *Chem. Phys. Lett.* **1996**, *261*, 35–44.
73. Stone, A. J. *The Theory of Intermolecular Forces*; Clarendon Press: Oxford, 1996.
74. Bowman, J. M.; Gazdy, B.; Schafer, P.; Heaven, M. C. *J. Phys. Chem.* **1990**, *94*, 2226–2229.
75. Kofranek, M.; Lischka, H.; Karpfen, A. *Chem. Phys.* **1988**, *121*, 137–153.
76. Quack, M.; Suhm, M. A. *J. Chem. Phys.* **1991**, *95*, 28–59.
77. Dykstra, C. E. *J. Phys. Chem.* **1990**, *94*, 180–185.
78. Klein, M. L.; McDonald, I. R. *J. Chem. Phys.* **1979**, *71*, 298–308.
79. Zhang, C.; Freeman, D. L.; Doll, J. D. *J. Chem. Phys.* **1989**, *91*, 2489–2497.
80. Honda, K.; Kitaura, K.; Nishimoto, K. *Bull. Chem. Soc. Japan* **1992**, *65*, 3122–3134.
81. Wright, D.; El-Shall, M. S. *J. Chem. Phys.* **1996**, *105*, 11199–11208.
82. Chałasiński, G.; Cybulski, S. M.; Szczęśniak, M. M.; Scheiner, S. *J. Chem. Phys.* **1989**, *91*,7048–7056.
83. Szczęśniak, M. M.; Chałasiński, G. *J. Mol. Struct. (Theochem)* **1992**, *261*, 37–54.
84. Szczęśniak, M. M.; Chałasiński, G. In *Molecular Interactions—From van der Waals to Strongly Bound Complexes*; Scheiner, S., Ed.; Wiley: New York, 1997, Chapter 2, pp 45–79.
85. Detrich, J.; Corongiu, C.; Clementi, E. *Chem. Phys. Lett.* **1984**, *112*, 426–430.
86. Quack, M.; Suhm, M. A. *Mol. Phys.* **1990**, *69*, 791–801.
87. Klopper, W.; Quack, M.; Suhm, M. A. *J. Chem. Phys.* **1998**, *108*, 10096-10115.
88. Simsek, M.; Yalçin, Z. *J. Math. Chem.* **1994**, *16*, 211–215.
89. Suhm, M. A. *Chem. Phys. Lett.* **1994**, *223*, 474–480.
90. Avoird, A. v. d.; Wormer, P. E. S.; Moszynski, R. *Chem. Rev.* **1994**, *94*, 1931–1974.
91. Bačić, Z.; Light, J. C. *Ann. Rev. Phys. Chem.* **1989**, *40*, 469–498.
92. Bowman, J. M.; Gazdy, B. *J. Chem. Phys.* **1990**, *93*, 1774–1784.
93. Bramley, M. J.; Carrington, Jr., T. *J. Chem. Phys.* **1993**, *99*, 8519–8541.
94. Zhang, D. H.; Wu, Q.; Zhang, J. Z. H.; von Dirke, M.; Bacic, Z. *J. Chem. Phys.* **1995**, *102*, 2315–2325.
95. Wu, Q.; Zhang, D. H.; Zhang, J. Z. H. *J. Chem. Phys.* **1995**, *103*, 2548–2554.
96. Bacic, Z.; Qiu, Y.; Zhang, J. Z. H.; Müller, H. B.; Quack, M.; Suhm, M. A. in preparation.
97. Zhang, D. H.; Zhang, J. Z. H. *J. Chem. Phys.* **1993**, *99*, 6624–6633.
98. Zhang, D. H.; Wu, Q.; Zhang, J. Z. H. *J. Chem. Phys.* **1995**, *102*, 124–132.
99. von Dirke, M.; Bacic, Z.; Zhang, D. H.; Zhang, J. Z. H. *J. Chem. Phys.* **1995**, *102*, 4382–4389.
100. Cohen, R. C.; Saykally, R. *Ann. Rev. Phys. Chem.* **1991**, *42*, 369–392.
101. Bramley, M. J.; Trump, J. W.; Carrington, Jr., T.; Corey, G. C. *J. Chem. Phys.* **1994**, *100*, 6175–6194.
102. Maynard, A. T.; Wyatt, R. E.; Iung, C. *J. Chem. Phys.* **1995**, *103*, 8372–8390.
103. Wyatt, R. E.; Iung, C.; Leforestier, C. *Acc. Chem. Res.* **1995**, *28*, 423–429.
104. Leforestier, C.; Braly, L. B.; Liu, K.; Elrod, M. J.; Saykally, R. J. *J. Chem. Phys.* **1997**, *106*, 8527–8544.
105. Quack, M.; Suhm, M. A. *Chem. Phys. Lett.* **1995**, *234*, 71–76.
106. Quack, M.; Suhm, M. A. *Theor. Chim. Acta* **1996**, *93*, 61–65.
107. Luckhaus, D.; Meyer, R.; Quack, M.; Suhm, M. A. to be published.
108. Luckhaus, D.; Müller, H. B.; Quack, M.; Suhm, M. A. in preparation.
109. Barton, A. E.; Howard, B. J. *Faraday Discuss. Chem. Soc.* **1982**, *73*, 45–62.
110. Marshall, M. D.; Jensen, P.; Bunker, P. R. *Chem. Phys. Lett.* **1991**, *176*, 255–260.
111. Schütz, M.; Klopper, W.; Lüthi, H.-P.; Leutwyler, S. *J. Chem. Phys.* **1995**, *103*, 6114–6126.
112. Althorpe, S. C.; Clary, D. C.; Bunker, P. R. *Chem. Phys. Lett.* **1991**, *187*, 345–353.
113. Quack, M.; Troe, J. *Ber. Bunsenges. Phys. Chem.* **1974**, *78*, 240–252.
114. Jung, J. O.; Gerber, R. B. *J. Chem. Phys.* **1996**, *105*, 10332–10348.
115. Jelski, D. A.; Haley, R. H.; Bowman, J. M. *J. Comp. Chem.* **1996**, *17*,1645–1652.

116. Bunker, P. R.; Carrington, Jr., T.; Gomez, P. C.; Marshall, M. D.; Kofranek, M.; Lischka, H.; Karpfen, A. *J. Chem. Phys.* **1989**, *91*, 5154–5159.
117. Bunker, P. R.; Jensen, P.; Karpfen, A.; Kofranek, M.; Lischka, H. *J. Chem. Phys.* **1990**, *92*, 7432–7440.
118. Quack, M.; Suhm, M. A. *Chem. Phys. Lett.* **1991**, *183*, 187–194.
119. Anderson, J. B. *J. Chem. Phys.* **1975**, *63*, 1499–1503.
120. Sun, H.; Watts, R. O. *J. Chem. Phys.* **1990**, *92*, 603–616.
121. Lester, Jr., W. A.; Hammond, B. L. *Ann. Rev. Phys. Chem.* **1990**, *41*, 283–311.
122. Suhm, M. A.; Watts, R. O. *Phys. Reports* **1991**, *204*, 293–329.
123. Hammond, B. L.; Lester, Jr., W. A.; Reynolds, P. J. *Monte Carlo Methods in Ab Initio Quantum Chemistry*; World Scientific: Singapore, 1994.
124. Ceperley, D. M.; Mitas, L. *Adv. Chem. Phys.* **1996**, *XCIII*, 1–38.
125. Kosztin, I.; Faber, B.; Schulten, K. *Am. J. Phys.* **1996**, *64*, 633–644.
126. Anderson, J. B. *J. Chem. Phys.* **1976**, *65*, 4121–4127.
127. Sandler, P.; Buch, V.; J., Sadlej, J.; *J. Chem. Phys.* **1996**, *105*, 10387–10397.
128. Klein, D. J.; Pickett, H. M. *J. Chem. Phys.* **1976**, *64*, 4811–4812.
129. Lewerenz, M.; Watts, R. O. *Mol. Phys.* **1994**, *81*, 1075–1091.
130. Caffarel, M.; Claverie, P.; Mijoule, C.; Andzelm, J.; Salahub, D. R. *J. Chem. Phys.* **1989**, *90*, 990–1002.
131. Barnett, R. N.; Sun, Z.; Lester, Jr., W. A. *Chem. Phys. Lett.* **1997**, *273*, 321–328.
132. Quack, M.; Troe, J. In *Encyclopedia of Computational Chemistry*; Wiley: New York, 1998. In press.
133. Cooley, J. W. *Math. Comput.* **1961**, *15*, 363–374.
134. Meyer, R. *J. Chem. Phys.* **1970**, *52*, 2053–2059.
135. Hollenstein, H.; Marquardt, R. R.; Quack, M.; Suhm, M. A. *J. Chem. Phys.* **1994**, *101*, 3588–3602.
136. Sandler, P.; Buch, V.; Clary, D. C. *J. Chem. Phys.* **1994**, *101*, 6353–6355.
137. Sandler, P.; oh Jung, J.; Szczesniak, M. M.; Buch, V. *J. Chem. Phys.* **1994**, *101*, 1378–1391.
138. Franken, K. A.; Dykstra, C. E. *J. Chem. Phys.* **1994**, *100*, 2865–2870.
139. Dykstra, C. E.; van Voorhis, T. A. *J. Comput. Chem.* **1997**, *18*, 702–711.
140. Meredith, A. W.; Ming, L.; Nordholm, S. *Chem. Phys.* **1997**, *220*, 63–78.
141. Coker, D. F.; Miller, R. E.; Watts, R. O. *J. Chem. Phys.* **1985**, *82*, 3554–3562.
142. Laurie, V. W.; Herschbach, D. R. *J. Chem. Phys.* **1962**, *37*, 1687–1693.
143. Ernesti, A.; Hutson, J. M. *Chem. Phys. Lett.* **1994**, *222*, 257–262.
144. Sorenson, J. M.; Gregory, J. K.; Clary, D. C. *Chem. Phys. Lett.* **1996**, *263*, 680–686.
145. Jorgensen, W. L. *J. Chem. Phys.* **1979**, *70*, 5888–5897.
146. Nemukhin, A. V.; Grigorenko, B. L. *Int. J. Quantum Chem.* **1997**, *62*, 55–65.
147. Car, R.; Parrinello, M. *Phys. Rev. Lett.* **1985**, *55*, 2471–2474.
148. Bueker, H.-H.; Helgaker, T.; Ruud, K.; Uggerud, E. *J. Phys. Chem.* **1996**, *100*, 15388–15392.
149. Lee, C.; Yang, W.; Parr, R. G. *Phys. Rev. B* **1988**, *37*, 785–789.
150. Becke, A. D. *J. Chem. Phys.* **1992**, *96*, 2155–2160.
151. Röthlisberger, U.; Parrinello, M. *J. Chem. Phys.* **1997**, *106*, 4658–4664.
152. Cheng, H.-P.; Barnett, R. N.; Landman, U. *Chem. Phys. Lett.* **1995**, *237*, 161–170.
153. Marx, D.; Parrinello, M. *J. Chem. Phys.* **1996**, *104*, 4077–4082.
154. Tschumper, G. S.; Yamaguchi, Y.; Schaefer III, H. F. *J. Chem. Phys.* **1997**, *106*, 9627–9633.
155. Davis, S.; Anderson, D. T.; Farrell, Jr., J. T.; Nesbitt, D. J. *J. Chem. Phys.* **1996**, *104*, 8197–8209.
156. Jensen, P.; Bunker, P. R.; Karpfen,, A.; Kofranek, M.; Lischka, H. *J. Chem. Phys.* **1990**, *93*, 6266–6280.
157. Chuang, C.-C.; Tsang, S. N.; Klemperer, W.; Chang, H.-C. *J. Phys. Chem. A.* **1997**, *101*, 6702–6708.
158. Mills, I. M. *J. Phys. Chem.* **1984**, *88*, 532–536.

159. Volobuev, Y.; Necoechea, W. C.; Truhlar, D. G. *J. Phys. Chem. A* **1997**, *101*, 3045–3048.
160. Necoechea, W. C.; Truhlar, D. G. *Chem. Phys. Lett.* **1996**, *248*, 182–188.
161. Huiszoon, C.; Briels, W. J. *Chem. Phys. Lett.* **1993**, *203*, 49–54.
162. Lewerenz, M. *J. Chem. Phys.* **1996**, *104*, 1028–1039.
163. Buch, V. *J. Chem. Phys.* **1992**, *97*, 726–729.
164. Gregory, J. K.; Clary, D. C. *J. Chem. Phys.* **1995**, *102*, 7817–7829.
165. Puttkamer, K. v.; Quack, M.; Suhm, M. A. *Infrared Phys.* **1989**, *29*, 535–539.
166. Quack, M. *Mol. Phys.* **1977**, *34*, 477–504.
167. Chang, H.-C.; Klemperer, W. *J. Chem. Phys.* **1996**, *104*, 7830–7835.
168. Davis, S.; Anderson, D. T.; Nesbitt, D. J. *J. Chem. Phys.* **1996**, *105*, 6645–6664.
169. Fraser, G. T. *J. Chem. Phys.* **1989**, *90*, 2097–2108.
170. Schuder, M. D.; Lovejoy, C. M.; Lascola, R.; Nesbitt, D. J. *J. Chem. Phys.* **1993**, *99*, 4346.
171. Sibert III, E. L. *J. Phys. Chem.* **1989**, *93*, 5022–5024.
172. Jensen, P.; Bunker, P. R.; Karpfen, A. *J. Mol. Spectrosc.* **1991**, *148*, 385–390.
173. Puttkamer, K. v.; Quack, M.; Suhm, M. A. *Mol. Phys.* **1988**, *65*, 1025–1045.
174. He, Y.; Müller, H. B.; Quack, M.; Suhm, M. A. In preparation.
175. Pine, A. S.; Howard, B. J. *J. Chem. Phys.* **1986**, *84*, 590–596.
176. Bohac, E. J.; Marshall, M. D.; Miller, R. E. *J. Chem. Phys.* **1992**, *96*, 6681–6695.
177. Farrell, Jr., J. T.; Suhm, M. A.; Nesbitt, D. J. *J. Chem. Phys.* **1996**, *104*, 9313–9331.
178. Oudejans, L.; Miller, R. E. *J. Phys. Chem. A.* **1997**, *101*, 7582–7592.
179. Hofacker, L. Z. *Naturforschg. A* **1963**, *18*, 607–619.
180. Gregory, J. K.; Whales, D. J.; Clary, D. C. *J. Chem. Phys.* **1995**, *102*,1592–1596.
181. Vasilev, G. K.; Makarov, E. F.; Chernyshov, Y. A.; Yakushev, V. G. *Sov. J. Chem. Phys.* **1987**, *4*, 1515–1527.
182. DeLeon, R. L.; Muenter, J. S. *J. Chem. Phys.* **1984**, *80*, 6092–6094.
183. Rensberger, K. J.; Copeland, R. A.; Robinson, J. M.; Crim, F. F. *J. Chem. Phys.* **1985**, *83*, 1132–1137.
184. Huang, Z. S.; Jucks, K. W.; Miller, R. E. *J. Chem. Phys.* **1986**, *85*, 3338–3341.
185. Fraser, G. T.; Pine, A. S. *J. Chem. Phys.* **1989**, *91*, 633–636.
186. Marshall, M. D.; Bohac, E. J.; Miller, R. E. *J. Chem. Phys.* **1992**, *97*, 3307–3317.
187. Bohac, E. J.; Miller, R. E. *J. Chem. Phys.* **1993**, *99*, 1537–1544.
188. Ewing, G. E. *J. Chem. Phys.* **1980**, *72*, 2096–2107.
189. Halberstadt, N.; Bréchignac, P.; Beswick, J. A.; Shapiro, M. *J. Chem. Phys.* **1986**, *84*, 170–175.
190. Pine, A. S. In Weber, A., Ed., *NATO ASI Series: Structure and Dynamics of Weakly Bound Molecular Complexes*; D. Reidel, 1987, pp 93–105.
191. Miller, R. E. *Science* **1988**, *240*, 447–453.
192. Yamada, K.; Winnewisser, M. *J. Mol. Spectrosc.* **1977**, *64*, 401–414.
193. Suhm, M. A. Dissertation, ETH Zürich, 1990.
194. Marquardt, R.; Quack, M.; Stohner, J.; Suhm, M. A. In *Supercomputing Projects Switzerland 1991/1992*; CSCS/EPFL/ETHZ, 1993, pp 31–34.
195. Quack, M. *Faraday Discuss. Chem. Soc.* **1981**, *71*, 309–311, 325–326, 359–364.
196. Andrews, L.; Davis, S. R.; Hunt, R. D. *Mol. Phys.* **1992**, *77*,993–1003.
197. Simons, J.; Hildebrand, J. H. *J. Am. Chem. Soc.* **1924**, *46*, 2183–2191.
198. Franck, E. U.; Meyer, F. Z. *Elektrochemie* **1959**, *63*, 571–582.
199. Janzen, J.; Bartell, L. S. *J. Chem. Phys.* **1969**, *50*, 3611–3618.
200. Strohmeier, W.; Briegleb, G. Z. *Elektrochemie* **1953**, *57*, 662, 668.
201. Kulcke, A. *Ber. – Max-Planck-Inst. Strömungsforsch.* **1994**, *13*, 1–160.
202. Huisken, F.; Kaloudis, M.; Kulcke, A.; Voelkel, D. *Infrared Phys. Technol.* **1995**, *36*, 171–178.
203. Huisken, F.; Tarakanova, E. G.; Vigasin, A. A.; Yukhnevich, G. V. *Chem. Phys. Lett.* **1995**, *245*, 319–325.
204. Huisken, F.; Kaloudis, M.; Vigasin, A. A. *Chem. Phys. Lett.* **1997**, *269*, 235–243.

205. Andrews, L.; Bondybey, V. E.; English, J. H. *J. Chem. Phys.* **1984**, *81*, 3452–3457.
206. Buck, U.; Meyer, H. *Phys. Rev. Lett.* **1984**, *52*, 109–112.
207. Stepanov, B. I. *Nature* **1946**, *157*, 808.
208. Vernon, M. F.; Lisy, J. M.; Krajnovich, D. J.; Tramer, A.; Kwok, H.-S.; Shen, Y. R.; Lee, Y. T. *Faraday Discuss. Chem. Soc.* **1982**, *73*, 387–397.
209. Huisken, F.; Kaloudis, M.; Koch, M.; Werhahn, O. *J. Chem. Phys.* **1996**, *105*, 8965–8968.
210. Michael, D. W.; Dykstra, C. E.; Lisy, J. M. *J. Chem. Phys.* **1984**, *81*, 5998–6006.
211. Botschwina, P.; Schulz, B.; Horn, M.; Matuschewski, M. *Chem. Phys.* **1995**, *190*, 345–362.
212. Astrand, P.-O.; Karlström, G.; Engdahl, A.; Nelander, B. *J. Chem. Phys.* **1995**, *102*, 3534–3554.
213. Beil, A.; Luckhaus, D.; Quack, M.; Stohner, J. *Ber. Bunsenges. Phys. Chem.* **1997**, *101*, 311–328.
214. Quack, M. *J. Chem. Soc. Faraday Discuss.* **1995**, *102*, 383–384.
215. Quack, M. *Il Nuovo Cimento* **1981**, *63B*, 358–377.
216. Laenen, R.; Rauscher, C. *J. Chem. Phys.* **1997**, *106*, 8974–8980.
217. Lagemann, R. T.; Knowles, C. H. *J. Chem. Phys.* **1960**, *32*, 561–564.
218. Franke, G.; Hilf, E. R.; Borrmann, P. *J. Chem. Phys.* **1993**, *98*, 3496–3502.
219. Wales, D. J.; Walsh, T. R. *J. Chem. Phys.* **1996**, *105*, 6957–6971.
220. Wales, D. J. *J. Am. Chem. Soc.* **1993**, *115*, 11191.
221. Liedl, K. R.; Sekušak, S.; Kroemer, R. T.; Rode, B. M. *J. Phys. Chem. A* **1997**, *101*, 4707–4716.
222. Loerting, T.; Liedl, K. R.; Rode, B. M. *J. Am. Chem. Soc.* **1998**, *120*, 404–412.
223. Chang, Y.-T.; Miller, W. H. *J. Phys. Chem.* **1990**, *94*, 5884–5888.
224. Suhm, M. A. *Chem. Phys. Lett.* **1993**, *214*, 373–380.
225. Varandas, A. J. C.; Marques, J. M. C. *J. Chem. Phys.* **1994**, *100*, 1908–1920.
226. Collins, M. A. *Adv. Chem. Phys.* **1996**, *XCIII*, 389–453.
227. Brown, D. F. R.; Gibbs, M. N.; Clary, D. C. *J. Chem. Phys.* **1996**, *105*, 7597–7604.
228. Adams, R. M.; Katz, J. J. *J. Opt. Soc. Amer.* **1956**, *46*, 895–898.
229. Kittelberger, J. S.; Hornig, D. F. *J. Chem. Phys.* **1967**, *46*, 3099–3108.
230. Atoji, M.; Lipscomb, W. N. *Acta Cryst.* **1954**, *7*, 173–175.
231. Johnson, M. W.; Sandor, E.; Arzi, E. *Acta Cryst. B* **1975**, *31*, 1998–2003.
232. Merkel, C.; Blumen, A. *Ber. Bunsenges. Phys. Chem.* **1977**, *81*, 1110.
233. Karpfen, A.; Yanovitskii, O. *J. Mol. Struct. (Theochem)* **1994**, *307*, 81–97.
234. Devlin, J. P.; Buch, V. *J. Phys. Chem. B* **1997**, *101*, 6095–6098.
235. Wales, D. J.; Doye, J. P. K. *J. Chem. Phys.* **1995**, *103*, 3061–3070.
236. Bartell, L. S. *J. Phys. Chem.* **1996**, *100*, 8197–8199.
237. Bartell, L. S.; Harsanyi, L.; Valente, E. J. *J. Phys. Chem.* **1989**, *93*, 6201–6205.
238. Barnes, J. A.; Gough, T. E.; Stoer, M. *Rev. Sci. Instr.* **1989**, *60*, 406–409.
239. Dunder, T.; Miller, R. E. *J. Chem. Phys.* **1990**, *93*, 3693–3703.
240. Disselkamp, R.; Ewing, G. E. *J. Chem. Phys.* **1993**, *99*, 2439–2448.
241. Bauerecker, S.; Taucher, F.; Weitkamp, C.; Cammenga, H. K. In *Proceedings of the SPIE: Application of Tunable Diode and Other Infrared Sources for Atmospheric Studies and Industrial Process Monitoring;* Fried, A., Ed.; SPIE, 1996, Vol. 2834, pp 257–261.
242. Felker, P. M.; Zewail, A. H. *Advances in Chemical Physics: Evolution of Size Effects in Chemical Dynamics 1* **1988**, *70*, 265–364.
243. Bingemann, D.; Gorman, M. P.; King, A. M.; Crim, F. F. *J. Chem. Phys.* **1997**, *107*, 661–664.
244. Woutersen, S.; Emmerichs, U.; Bakker, H. J. *J. Chem. Phys.* **1997**, *107*, 1483–1490.
245. Gregory, J. K.; Clary, D. C.; Liu, K.; Brown, M. G.; Saykally, R. J. *Science* **1997**, *275*, 814–817.
246. Bemish, R. J.; Chan, M. C.; Miller, R. E. *Chem. Phys. Lett.* **1996**, *251*, 182–188.
247. Howard, B. J.; Dyke, T. R.; Klemperer, W. *J. Chem. Phys.* **1984**, *81*, 5417–5425.
248. Fehrensen, B.; Luckhaus, D.; Quack, M. *Z. Physik. Chem.* **1998**. In press.
249. Quack, M. *J. Mol. Struct.* **1995**, *347*, 245–266.